Sodium alginate/polycaprolactone co-axial wet-spun microfibers modified with *N*-carboxymethyl chitosan and the peptide AAPV for *Staphylococcus aureus* and human neutrophil elastase inhibition in potential chronic wound scenarios

Catarina S. Miranda [a], A. Francisca G. Silva [b], Catarina L. Seabra [c], Salette Reis [c], M. Manuela P. Silva [b], Sílvia M.M.A. Pereira-Lima [b], Susana P.G. Costa [b], Natália C. Homem [d], Helena P. Felgueiras [a,*]

[a] *Centre for Textile Science and Technology (2C2T), University of Minho, Campus of Azurém, 4800-058 Guimarães, Portugal*
[b] *Centre of Chemistry (CQ), University of Minho, Campus of Gualtar, 4710-057 Braga, Portugal*
[c] *Associate Laboratory for Green Chemistry (LAQV), Network of Chemistry and Technology (REQUIMTE), Department of Chemical Sciences, Faculty of Pharmacy, University of Porto, 4050-313 Porto, Portugal*
[d] *Digital Transformation CoLab (DTx), Building 1, University of Minho, Campus of Azurém, 4800-058 Guimarães, Portugal*

ARTICLE INFO

ABSTRACT

In chronic wound (CW) scenarios, *Staphylococcus aureus*-induced infections are very prevalent. This leads to abnormal inflammatory processes, in which proteolytic enzymes, such as human neutrophil elastase (HNE), become highly expressed. Alanine-Alanine-Proline-Valine (AAPV) is an antimicrobial tetrapeptide capable of suppressing the HNE activity, restoring its expression to standard rates. Here, we proposed the incorporation of the peptide AAPV within an innovative co-axial drug delivery system, in which the peptide liberation was controlled by *N*-carboxymethyl chitosan (NCMC) solubilization, a pH-sensitive antimicrobial polymer effective against *Staphylococcus aureus*. The microfibers' core was composed of polycaprolactone (PCL), a mechanically resilient polymer, and AAPV, while the shell was made of the highly hydrated and absorbent sodium alginate (SA) and NCMC, responsive to neutral-basic pH (characteristic of CW). NCMC was loaded at twice its minimum bactericidal concentration (6.144 mg/mL) against *S. aureus*, while AAPV was loaded at its maximum inhibitory concentration against HNE (50 μg/mL), and the production of fibers with a core-shell structure, in which all components could be detected (directly or indirectly), was confirmed. Core-shell fibers were characterized as flexible and mechanically resilient, and structurally stable after 28-days of immersion in physiological-like environments. Time-kill kinetics evaluations revealed the effective action of NCMC against *S. aureus*, while elastase inhibitory activity examinations proved the ability of AAPV to reduce HNE levels. Cell biology testing confirmed the safety of the engineered fiber system for human tissue contact, with fibroblast-like cells and human keratinocytes maintaining their morphology while in contact with the produced fibers. Data confirmed the engineered drug delivery platform as potentially effective for applications in CW care.

1. Introduction

Chronic wounds (CW) are responsible for chronic pain and loss of mobility, while also increasing the risk of patient mortality. It is estimated that 1 to 2 % of the developed countries' population will be afflicted with CW at some point in their lifetime; hence, urgent steps must be taken to develop more effective managing and treating therapeutic strategies for CW care [1].

As an injury occurs, an inflammatory process takes place, during which the extracellular matrix (ECM) instigates the production of

platelet-derived factors. As a result, extrinsic and intrinsic coagulation pathways are stimulated, forming a reservoir of cytokines and growth factors. Neutrophils infiltrate the wound site and secrete reactive oxygen species (ROS) and proteases, in order to eliminate bacteria and remove products of damaged cells, also releasing other growth factors and cytokines [2]. In acute wounds, these processes are divided in four main stages: (1) hemostasis, involving the constriction of blood vessels, followed by the activation of a coagulation cascade and formation of a clot; (2) coagulation/inflammatory phase, resulting in blood vessels dilation, allowing white blood cells, growth factors, enzymes and nutrients to get to the wound site, raising exudates production; (3) proliferative phase, concerning the granulated tissue formation, composed of collagen and ECM; and (4) matrix remodeling, involving conversion of collagen type III into type I responsible for the regression and decrease of the number of blood vessels at the wound site. Unlike acute wounds, CW does not follow the wound healing steps nor spend equal periods of time in each step. CW present higher protease activity and pro-inflammatory cytokines than other wound types, triggering an abnormal inflammatory response. Moreover, bacterial infections are more common in CW, causing the degradation of the underlying tissue at the wound site. In infected scenarios, neutrophils secrete high amounts of cytokines and proteases, including neutrophil elastase (HNE), an enzyme responsible for the degradation of ECM and plasma proteins, in an attempt to destroy the microbials present, leading to several dysregulations, namely increase of local necrotic tissue and poor vascularization [3].

Bacterial infections induced by *Staphylococcus aureus* bacteria are responsible for high mortality and morbidity rates and are considered a major global health problem [3]. Indeed, nowadays, *S. aureus* is regarded as one of the most dangerous pathogens to human health by the World Health Organization (WHO). Statistics reveal that, in the United States of America (USA), the annual incidence of such infections is of 38.2 to 45.7 per 100.000 person-years (2015) [4]. In European countries, 150.000 *S. aureus* infections occur every year, causing at least 7.000 deaths (2015) [5]. Although antibiotics have been commonly administered to treat bacterial infections for many years, their excessive consumption has led to an increase in the number of antibiotic-resistant microorganisms, raising the need for alternatives. Antimicrobial peptides (AMPs) consist of low molecular weight molecules with an overall positive charge and are highly effective against Gram-positive and Gram-negative bacteria as well as fungi and viruses [6]. According to Homem et al., AMPs generally act by disrupting the bacteria cell membrane integrity by establishing electrostatic interactions between the negatively charged bacteria wall and the positively charged AMPs or by altering the microbials' lipid bilayer structure [7]. Many AMPs are also known to possess the ability to promote re-epithelization, granulation tissue formation, and ECM synthesis. The tetrapeptide Ala-Ala-Pro-Val (AAPV) has been proven effective in inhibiting the action of HNE, an enzyme that, in CW inflammatory scenarios, registers an abnormally high activity. According to Santos et al., in such conditions, HNE reaches 10–40 times the amount detected in acute wounds, causing degradation of endogenous and supplemental growth hormones [8]. The hydrophobic sequences present in the AAPV resemble amino acid regions in elastin (a protein susceptible to HNE activity). This way, the tetrapeptide can bind to subsites of HNE, inhibiting the enzyme competitively. However, AMPs face limitations to their generalized use, namely low bioavailability and stability in physiological media, potential toxicity (require large concentrations), and sensitivity to variations in environmental conditions, to name a few. To overcome such challenges, AMPs can be incorporated within polymeric carriers, like co-axial fiber-based constructs, which protect the active agent and guarantee that its biological activity is not lost, aside from controlling its localized, sustained delivery [8].

Wet-spinning is a technique in which a polymeric solution is injected into a coagulation bath composed of a non-solvent or a poor solvent of that polymer. As the solution reaches the coagulation bath, precipitation occurs and solid fibers can be generated. Wet-spun fibers tend to present

high porosity and may be constructed with many levels of organization, enabling cell permeation and infiltration [9]. In this study, *co*-axial wet-spun fibers were produced with a core composed of polycaprolactone (PCL), a synthetic polymer that presents excellent mechanical properties, intended to maintain the fibers' structural integrity [10], mixed with AAPV, for local enzymatic activity regulation. The shell was made of a blend of sodium alginate (SA), a natural biodegradable polymer with high swelling capacities, which purpose was to control local moisture and absorb exudates [11], and *N*-carboxymethyl chitosan (NCMC), a non-toxic and biodegradable chemically synthesized derivative of chitosan (CS), responsive to neutral-to-basic pH, which endowed fibers with antibacterial activity against *S. aureus*. Two mechanisms of antibacterial action have been suggested for CS: electrostatic stacking at the bacteria cell surface, interfering with the bacterial metabolism, and the blockage of RNA transcription from DNA, by the adsorption of penetrated CS to DNA molecules. Considering CS is water insoluble, NCMC, in which the free amino group is replaced by a carboxymethyl group for enhanced water affinity, was here explored [12]. The NCMC solubility in neutral-basic pH, characteristic of CW environments, was expected to guarantee a controlled access to the fibers' core and, thus, a paced liberation of AAPV. HNE inhibition evaluations were conducted to establish the AAPV's maximum inhibitory concentration (IC_M), while NCMC was subjected to antimicrobial testing to determine its minimum bactericidal concentration (MBC) against *S. aureus*. Wet-spun fibers modified with AAPV and NCMC, envisioned for a 24-hour application period, were characterized by brightfield and scanning electron microscopy (SEM) for their morphology, and by Fourier-transform infrared spectroscopy (FTIR) and differential scanning calorimetry (DSC) for confirming the presence of the four elements (PCL, AAPV, SA and NCMC) within the co-axial structures. Elongation at break, swelling and degradation studies were conducted to establish the fibers resilience over time. Finally, AAPV and NCMC controlled release monitoring, and bacteria and cell biology testing were carried out to verify the fibers biological potential. To the authors' knowledge, this is the first report on the production of co-axial wet-spun fibers loaded with AAPV and NCMC for treating CW. Although there are still not many reports on co-axial wet-spun fibers for wound healing applications, in the future it is expected research to e*v*olve towards that direction.

2. Materials and methods

2.1. Materials

SA (from brown algae, medium viscosity), PCL (Mw 80,000), CS (Mw 100–300 kDa), ethyl cyanoglyoxylate-2-oxime (Oxyma), 1,3-diisopropylcarbodiimide (DIC), dichloromethane (DCM), chloroacetic acid, deuterium oxide (D_2O), elastase from human leukocytes, trypsin inhibitor from soybean, N-Methoxysuccinyl-Ala-Ala-Pro-Val-p-nitroanilide (N-MeO-Suc-Ala-Ala-Pro-Val-p-NA), Dulbecco's Modified Eagle Medium (DMEM, high glucose, GlutaMAX, pyruvate)Penicillin-streptomycin (10,000 U/mL), Trypsin-EDTA (0.25 % w/v) were purchased from Gibco Life Technologies (California, USA), Fetal Bovine Serum (FBS) was purchased from Biowest (Missouri, USA), Trypan blue, Sodium resazurin, Triton X-100 were purchased from Sigma-Aldrich (St. Louis, Missouri, USA) and Hoechst 33342 was purchased from Invitrogen Thermo Fisher Scientific Corporation (Massachusetts, USA). Lactate dehydrogenase (LDH) cytotoxicity detection kit was obtained from Takara Bio Inc. (Shiga, Japan). 2-chlorotritylchloride resin and 9-fluorenylmethyloxyicarbonyl-aminoacids (Fmoc-AA) were acquired from AAPPTec Peptide (Louisville, USA). *N,N*-dimethylformamide (DMF), acetic acid (AcOH), acetonitrile (ACN), piperidine, 9-fluorenyl-methyloxicarbonyl (Fmoc), dichloromethane, sodium hydroxide (NaOH), sodium carbonate (Na_2CO_3), 2,2,2-trifluoroethanol (TFE) and trifluoroacetic acid (TFA) were acquired from Merck (Darmstadt, Germany). Dimethyl sulfoxide (DMSO) was acquired from Fisher (Maharashtra, India). Calcium chloride ($CaCl_2$, anhydrous) was employed as

coagulation/crosslinking agent during wet-spinning and was supplied from Chem-Lab (Zedelgem, Belgium). Tris-hydrochloride (Tris-HCl) was purchased from Roche (Basel, Switzerland).

Sodium phosphate dibasic (Na_2HPO_4, Sigma-Aldrich), monosodium phosphate monohydrate (NaH_2PO_4, Merck) and sodium chloride (NaCl, Merck) were used in the preparation of phosphate buffer saline solution (PBS at 0.1 M: 1.44 g/L of Na_2HPO_4, 0.24 g/L of KH_2PO_4, 0.20 g/L KCl and 8.00 g/L of NaCl, adjusted to physiological pH 7.4). Gram-positive bacterium *S. aureus* (ATCC 6538) was supplied by American Type Culture Collection (ATCC, Virginia, USA). For bacteria growth, trypticase soy broth (TSB) and trypticase soy agar (TSA) were purchased from VWR (Alfragide, Portugal), while mueller hinton broth (MHB) was obtained from CondaLab (Madrid, Spain). All reagents were used without further purification.

Mouse fibroblast cell line (L929) was purchased from the European Collection of Authenticated Cell Cultures (ECACC, Salisbury, UK) and the human keratinocytes cell line (HaCaT) was purchased from Cell Lines Service GmbH (CLS, Eppelheim, Germany).

2.2. Synthesis and characterization of Ala-Ala-Pro-Val (AAPV) and Fmoc-Ala-Ala-Pro-Val (Fmoc-AAPV)

The AAPV peptide was prepared by solid phase peptide synthesis, using a 2-chlorotritylchloride resin pre-loaded with *valine* (0.53 mmol/g functionalization). The coupling steps were carried out using Fmoc amino acids (5.0 eq. relatively to the resin functionalization), DIC (5.5 eq.) and ethyl cyanoglyoxylate-2-oxime (Oxyma) (5.5 eq.) in dry DMF and 6 h of stirring at room temperature (RT). After each coupling, the Fmoc group was removed with 20 % piperidine in DMF and the resin was washed with DMF (3×) and MeOH (3×). This washing cycle was repeated four times. The separation of the peptide from the resin was performed with the cleavage cocktail AcOH/TFE/DCM at 1/2/7 (v/v/v).

The peptide was precipitated from the reaction mixture with cold diethyl ether, centrifuged and dried. The Fmoc-AAPV peptide was prepared similarly to AAPV with the exception that the last Fmoc group was not removed prior to the separation of the peptide from the resin, with the peptide being precipitated from the reaction mixture with cold diethyl ether and petroleum ether.

The peptides' purity was checked by analytical High-Performance Liquid Chromatography (HPLC) using a Lichroscoper RP-18 column, pump Jasco PU-980, UV-975 detector and Shimadzu C-R6A chromato-pac from Elsichrom (Valloxvagen, Sweden). TFA and an ACN/distilled water (dH₂O) mixture at 1/1 (v/v), with 0.1 % (v/v) TFA were used as eluent for AAPV and Fmoc-AAPV, respectively, and the peptides detected at 214 nm. The peptides' structure was confirmed with ¹H and ¹³C Nuclear Magnetic Resonance Spectroscopy (NMR, Bruker Avance III 400, Switzerland), using 20 μL TFA per mL of DMSO-d_6 as solvent.

2.3. Synthesis and characterization of NCMC

NCMC was synthesized according to Song et al. [12]. Briefly, 7.5 g of chloroacetic acid were dissolved in 30 mL of dH₂O, with the solution pH being adjusted to 7.0 with 3 M NaOH aqueous solution. 1.5 g of CS, previously dried overnight at 50 °C, were then added to the mixture, which was heated to 90 °C. During 4 h, the pH was adjusted to 7.0, every 30 min, using 20 % w/v Na_2CO_3. The solution was diluted in dH₂O (1/1 v/v) and filtrated using Whatman n° 4 filter paper. Afterwards, 95 % v/v ethanol was added to the recovered filtrate solution (1/3 v/v), which was centrifugated twice for 10 min at 4000 rpm. The supernatant was discarded between centrifugations and replaced by new 95 % v/v ethanol. Finally, pure ethanol was added to the collected precipitates and the content was again filtered. The precipitate was dried at 37 °C overnight. The NCMC degree of substitution (DS) was determined using the potentiometric titration method reported by Ge et al. [13], and its structure was confirmed by NMR, using D₂O as solvent (as reported in

Section 2.2). FTIR analysis was also conducted, comparing NCMC spectra with pure CS FTIR spectra to confirm the modification at the CS amine groups (wavenumbers ranging between 400 and 4000 cm⁻¹, 200 scans being performed at 2 cm⁻¹ resolution).

2.4. Determination of minimum inhibitory and bactericidal concentrations (MIC and MBC) of AAPV and NCMC

AAPV and NCMC MICs against *S. aureus* were determined using the broth microdilution method [14], which adapts the standard published by the Clinical and Laboratory Standards Institute (CLSI) and the European Committee on Antimicrobial Susceptibility Testing (EUCAST) [15].

Stock solutions of AAPV and NCMC were prepared at concentrations of 4.096 mg/mL and of 10.240 mg/mL in dH₂O, respectively. 100 μL of each solution were added to the first column of a 96-well plate (in triplicate). Subsequently, serial dilutions (1/2 v/v) were performed in MHB, reaching a final volume of 50 μL in each well. The bacterium suspension prepared in MHB at 1×10^6 colony forming units (CFUs)/mL was then added to the wells (50 μL; final bacterium concentration of 5×10^5 CFUs/mL). As control, MHB (negative) and the bacterium suspension free from AAPV/NCMC (positive) were used. Absorbances were read with an EZ READ 2000 Microplate Reader (Biochrom, Cambridge, UK) at 600 nm, before and after the 24 h incubation period at 37 °C and 120 rpm. MIC was identified by differences in absorbance readings. The MBC was determined by culturing the bacterium solution at MIC and its vicinities (before and after MIC value). To accomplish that, aliquots were collected, serially diluted in PBS (10^1 to 10^4), plated in TSA, and then incubated at 37 °C for 24 h, at which point grown colonies were observed and counted.

2.5. HNE inhibitory assay

HNE activity and its inhibition by AAPV were determined following an adapted version of the procedure described by Melzig et al. [16]. Briefly, 125 μL of substrate solution (N-MeO-Suc-Ala-Ala-Pro-Val-p-NA dissolved in Tris-HCl buffer, pH 7.5) were added to 405 μL of 0.1 M Tris-HCl. Then, 50 μL of testing solutions, consisting of AAPV at concentrations between 0.10 and 200.00 μg/mL in Tris-HCl buffer (pH 7.5), were added to the mixture. 20 μL of enzyme solution (HNE diluted in Tris-HCl buffer at 45 mU) were combined with the mixture and *vortexed* for 1 min, prior to incubation at 37 °C for 1 h; in CW, HNE is present at concentrations between 36 and 54 mU/mL [17]. In the end, 500 μL of soybean trypsin inhibitor prepared in Tris-HCl buffer were added to stop the reaction, and absorbances were read at 405 nm, using an EZ Read 2000 Microplate Reader. Samples without the testing peptide were used as controls. Experiments were conducted in triplicate, with three absorbance readings being done per replicate (mean averaging nine measurements). Data were reported in IC_M, the concentration that guarantees maximum HNE inhibition.

2.6. Wet-spun fibers production

2 % w/v SA and 10 % w/v PCL solutions were prepared for 3 h in dH₂O and for 1 h in DMF, respectively, both stirred continuously at 50 °C. NCMC was added to a portion of the SA solution at $2 \times$ MBC in dH₂O and homogeneously blended for 1 h at 50 °C (SA-NCMC solution). On its turn, AAPV was combined with the PCL solution cooled at RT (to prevent peptide denaturation) at IC_M in DMF and left to homogenize for 1 h at RT (PCL-AAPV solution). Viscosities were measured using a viscometer Brookfield DV-II + Pro (Boston, USA), spindle 21, with speeds of 5–40 rpm and temperature of 16–30 °C. All solutions were ultrasonicated using a J.P.Selecta Ultrasons-HD 5 L (Barcelona, Spain), to remove air bubbles prior to fiber production. The wet-spinning setup was composed of two syringe pumps (NE-300, New Era Pump Systems, Norleq, Santo Tirso, Portugal), to control the rate and volume of

extrusion, a co-axial spinneret and a large tray containing the 2 % w/v CaCl₂ coagulation bath, at RT. All fibers were collected manually, dried for 1 h at RT and washed for 10 min in dH₂O for coagulation bath salt elimination. Syringes connected to the inner port (core) and the outer port (shell) of the co-axial spinneret were loaded with PCL-AAPV solution and SA-NCMC solution, respectively. PCL-AAPV was extruded at 0.10 mL/min, whereas SA-NCMC was extruded at 0.15 mL/min, forming SA-NCMC-PCL-AAPV fibers. Control fibers were produced without the shell (PCL and PCL-AAPV), without the core (hollow fibers of SA and SA-NCMC) and without some of the components of the co-axial system, namely NCMC and AAPV (SA-PCL), NCMC (SA-PCL-AAPV), and AAPV (SA-NCMC-PCL). Processing parameters for control samples were equal to those of the complete system. In the end, they were stored in a cabinet desiccator (Sicco, Grünsfeld, Germany) at 19 °C and a relative humidity of 41 %, for further testing. Microfibers were developed to sustain a 24 h period of contact with a prospective wound.

2.7. Microfibers' physical, chemical, thermal and mechanical characterization

2.7.1. Brightfield microscopy

The fibers' morphology was assessed by brightfield microscopy using an inverted Leica DM IL LED microscope (Leica microsystems, Wetzlar, Germany). Five images were collected at 5× and 10× magnifications, and the average fiber thicknesses (5 measurements per image) were determined via ImageJ® software (version 1.53, National Institutes of Health, Bethesda, Maryland, USA).

2.7.2. Scanning electron microscopy (SEM)

Micrographs were collected by using a dual column ultra-high resolution field emission SEM (NOVA 200 Nano SEM, FEI Company, Texas, USA) with 10 kV of accelerating voltage. Samples were initially coated with a 10 nm film of gold-palladium (Au-Pd, 80–20 % w/v), using a 208 High-Resolution Sputter-Coater (Cressington Company, Watford WD19 4BX, UK) coupled to an MTM-20 High-Resolution Thickness Controller (Cressington Company). Images were collected with a magnification of 500× and processed with Image J® software.

2.7.3. Attenuated total reflectance-Fourier transform infrared spectroscopy (ATR-FTIR)

The surface chemistry and chemical composition of the fibers were analyzed by ATR-FTIR using an IRAffinity-1S (Shimadzu, Kyoto, Japan), coupled with a HATR 10 accessory containing a diamond crystal. Spectra were obtained in wavenumbers ranging between 400 and 4000 cm⁻¹, with 200 scans being performed at 2 cm⁻¹ resolution.

2.7.4. Differential scanning calorimetry (DSC)

DSC analyses were conducted using a Mettler Toledo-equipment model DSC-821e equipment (Columbus, USA) coupled to a cooling accessory (Labplant cryostat RP-60, Huddersfield, UK). Samples were placed in an aluminum crucible (Mettler Toledo, ME-26763, Columbus, USA) and were exposed to a heating rate of 10 °C/min, from 25 to 450 °C, under argon atmosphere at 35 mL/min. Assays were performed using as reference an empty crucible.

2.7.5. Mechanical performance

The maximum elongations at break of the wet-spun fibers were determined using a Housefield H5KS dynamometer (Artilab, Kerkdriel, Netherlands), associated with the QMAT Materials Testing & Analysis software, following the standard ISO 2062 - 2009. Filaments of 10 cm in length were analyzed at RT with a holding distance, also known as gauge length, starting at 100 mm, which continuously increased until reaching the fibers' maximum elongation at break. The crosshead speed was established at 25 mm/min, using a loading cell of 2.5–250.0 N, applied with a load range of 5 N and a pre-load of 0 N.

2.7.6. Degree of swelling (DS)

The fibers DS was assessed in PBS at 37 °C. 10 mg samples were weighted before and after 24 h immersion (at which point saturation was reached). DS was determined using the following expression (Eq. (1)):

$$DS\ (\%) = \frac{ws - wd}{wd} \times 100, \tag{1}$$

in which ws (mg) represents the weight of the swollen fibers (wet state) after each incubation period and wd (mg) represents the weight of the fibers in their dried state, prior to PBS immersion.

2.7.7. Fiber degradation

The fibers degradation profile was assessed in PBS by incubating 10 mg samples of each type of fiber, at 37 °C for up to 28 days. Media were exchanged every week. After 1, 3, 7, 14, 21 and 28 days of incubation, samples were weighted. Mass loss was determined using the following expression (Eq. (2)):

$$mass\ loss\ (\%) = \frac{mi - mf}{mi} \times 100, \tag{2}$$

in which mi (mg) represents the weight of the hydrated fibers at time 0 h (fibers were initially hydrated in dH₂O, until saturation) and mf (mg) corresponds to the fibers' weight after each incubation period.

2.8. AAPV and NCMC release kinetics

A chemically modified version of AAPV (Fmoc-AAPV) was used in this assay, since an overlapping of maximum absorbances between all fiber compounds was observed, making it impossible for AAPV release kinetics tracking. This way, by including a fluorescent group (Fmoc), it was possible to monitor the release by fluorimetry.

An Fmoc-AAPV calibration curve in PBS at concentrations between 0.010 and 0.500 μg/mL was elaborated using a Fluoromax-4 Spectrofluorometer 384 TC (Horiba Jobin Yvon, USA) and FluorEssence software. Fmoc-AAPV-loaded fibers were immersed in PBS for 1, 2, 4, 6 and 24 h of incubation at 37 °C and 120 rpm, and aliquots of 150 μL were collected at each time point. Absorbances were then read in the range 290–400 nm. Differences in absorbance between Fmoc-AAPV-loaded and unloaded fibers were established to eliminate SA and/or PCL influence on the release profiles. Results were reported as absorbance vs wavenumber.

Release kinetics of NCMC could not be evaluated due to an overlap of maximum absorbances with both SA and PCL. Modification of NCMC with fluorescent components was also impossible as polymer viscosity altered, conditioning significantly fibers wet-spinning and, thus, modifying the original processing parameters and the fibers' physical and mechanical properties.

2.9. Fibers' inhibitory effect against HNE

AAPV-loaded fibers were incubated in PBS at 37 °C and 120 rpm for 1, 2, 4, 6 and 24 h. After each incubation period, aliquots of 150 μL were collected; these represented the testing solutions. HNE inhibition experiments were conducted as reported in Section 2.5. Absorbances were read at 405 nm (EZ Read 2000 Microplate Reader) and data were reported as IC$_M$. Experiments were conducted in triplicate, with three absorbance readings being done per replicate (mean averaging nine measurements).

2.10. Bacteria inhibition: time-kill kinetics

Time-kill kinetics tests were conducted according to standard ASTM E2149-01, adapted as reported by Homem et al. [18]. The antibacterial profile of the wet-spun fibers was evaluated against a 1 × 10⁵ CFUs/mL

S. aureus suspension in TSB. Samples of 10 mg were immersed in 1 mL of bacterium suspension and incubated at 37 °C and 120 rpm for 1, 2, 4, 6 and 24 h. At each time point, bacteria suspensions were serially diluted in PBS (10^1 to 10^4), plated in TSA, and incubated at 37 °C for 24 h. Grown colonies were counted, and results were expressed in log reduction and number of surviving colonies (CFUs/mL). All measurements were performed in triplicate (three measurements were done per replicate, with data averaging nine values) and data were processed using the GraphPad Prism 8.0 software. In addition, bacteria viability was examined using the LIVE/DEAD® BacLight™ Bacterial Viability Kit L13152, with SYTO 9 and propidium iodide staining reagents, respectively for live and dead bacteria colonies labelling.

2.11. Cytocompatibility testing

2.11.1. Cell culture conditions

The cytocompatibility and cell proliferation of all fiber typologies towards mouse fibroblast cell line (L929) and human keratinocytes cell line (HaCaT) were evaluated using direct contact assay. The cytocompatibility testing (metabolic activity and cell lysis analyses) was performed according to the international standard ISO 10993-5:2009. Cells were thawed and sub-cultured in DMEM medium supplemented with 10 % (v/v) inactivated FBS (30 min, 56 °C) and 1 % v/v penicillin-streptomycin, at 37 °C in a humidified atmosphere of 5 % CO_2, until reaching 90 % confluence. Thereafter, cells were chemically detached from cell culture flasks using trypsin-EDTA at 0.25 % w/v. The number of cells was determined using a Neubauer Chamber, labelling cells with trypan blue (ratio 1/1) and cells were counted using a Motic® Inverted Microscope (Motic, Barcelona, Spain). Cells were seeded in 96-well tissue culture polystyrene (TCPS, VWR®, Pennsylvania USA) plates, at the density of 5×10^4 cells per well, and incubated for 24 h at 37 °C in a humidified atmosphere of 5 % CO_2. The experiments were performed using fibroblast cells in passage 10–15 and keratinocytes cells line in passage 20–25.

2.11.2. Cell viability assessment

After 24 h of incubation, the metabolic activity of the cells was evaluated by resazurin staining. Briefly, 0.01 mg/mL of sodium resazurin in medium solution was added to the wells and incubated for 2 h at 37 °C and 5 % CO_2 atmosphere. Afterwards, 100 μL of supernatant were transferred to a black 96-well plate (Falcon®, Arizona, USA) and the fluorescence was measured ($\lambda ex = 560$ and $\lambda em = 590$ nm) using a microplate fluorometer (Cytation 5 Cell Imaging Reader - BioTek Instruments, Vermont, USA). The percentage of metabolic activity was evaluated by Eq. (3) as an indicator of cells viability:

$$\text{Metabolic activity } (\%) = \frac{\text{Flu}_s - \text{Flu}_{nc}}{\text{Flu}_{pc} - \text{Flu}_{nc}} \times 100, \tag{3}$$

where the Flu_s is the fluorescence of the samples, Flu_{nc} is the fluorescence of the negative control, the untreated cells, and Flu_{pc} is the fluorescence of the positive control, the treated cells with 2 % v/v Triton X-100 solution.

2.11.3. Cell lysis assessment

Cell lysis was evaluated using lactate dehydrogenase (LDH) assay, according to the manufacturer. After 24 h incubation of cells with all fiber typologies, plates were centrifuged at 250*g* for 10 min (Centrifuge 5810R, Eppendorf®, Hamburg, Germany) and the supernatant was collected to a new 96-well plate. Then, LDH cytotoxicity detection kit was added at 1/1 v/v ratio and incubated at RT for 15 min, protected from light. The absorbance was read at 490 nm and 690 nm in a plate reader (Cytation 5 Cell Imaging Reader- BioTek Instruments, Vermont, USA). The cell lysis by LDH release into the cell culture medium was calculated by Eq. (4):

$$\text{Cell lysis } (\%) = \frac{\text{Abs}_s - \text{Abs}_{nc}}{\text{Abs}_{pc} - \text{Abs}_{nc}} \times 100, \tag{4}$$

where the Abs_s is the absorbance of the samples, Abs_{nc} is the absorbance of negative control that are treated cells with 2 % (v/v) Triton™ X-100 solution, and Abs_{pc} is the fluorescence of positive control that are untreated cells.

2.12. Cell proliferation by Hoechst staining

Cell proliferation was evaluated by exposing fibers in direct contact with cells for 1 and 2 days. The cells were stained with Hoechst 33342 at 0.1 μg/mL for proliferative profile evaluation. The positive control group (non-exposed cells to fibers), negative control (cells exposed to DMSO) and the fibers' control group were stained with Hoechst as well. The calibration curve was performed by cell counting and the fluorescence measurement of cell nuclei (Fluorescence = 0.0033 [Cell] + 466.39, $R^2 = 0.992$ for L929; Fluorescence = 0.0021 [Cell] + 449.83, $R^2 = 0.996$ for HaCaT). The cell nuclei were read at 361 nm and 497 nm (Cytation 5 Cell Imaging Reader, − BioTek Instruments, Vermont, USA). Cell concentration was determined using the calibration curves prepared for L929 and HaCaT.

2.13. Cell morphology observation by brightfield microscopy

Cells were visualized at brightfield using an optical microscope. Light microscope images were obtained at the beginning of the experiment (t = 0 h) and after 24 h of incubation in contact with the samples, as to evaluate the cell morphology and the possible presence of damaged areas. The images were acquired at a $10\times$ magnification objective of 0.25 N.A. using a Motic ™ Camera S12 coupled with Motic Image Plus 3.0 software (Motic, Barcelona, Spain).

2.14. Statistical analysis

All measurements were conducted in triplicate unless otherwise referred in the experimental sections. Numerical data were reported as mean ± standard deviation (SD). Data were treated using GraphPad Prism 8.0 Software (GraphPad Software Inc., USA). Normality analysis was performed, and results were analyzed using One-way ANOVA, Dunnett and Tukey tests. Statistically significant differences were considered at $p < 0.05$.

3. Results and discussion

3.1. AAPV synthesis and characterization

The AAPV peptide was prepared by solid phase peptide synthesis using a 2-chlorotritylchloride resin pre-loaded with valine. AAPV was obtained as a white powder solid with ≈94 % yield (≈0.131 g). A purity of ≈98 % was estimated by analytical HPLC, with a retention time of 4.49 min (Fig. S1 in Supporting Information). For such purpose, 1 mg of AAPV was dissolved in 100 μL of eluent and tested with a flow of 0.6 mL/min at 214 nm. with an ACN/dH$_2$O (1/4 v/v) with 0.1 % TFA mixture as eluent. The peptide structure was confirmed by ^{1}H and ^{13}C NMR spectroscopy using DMSO-d_6 combined with TFA as solvent, corroborating data from previous reports (Section S1 – NMR Signals, in Supporting Information) [19].

The peptide's antibacterial properties were evaluated for the first time against the Gram-positive bacterium *S. aureus*. The MIC/MBC was established at 2.048 mg/mL. AAPV antibacterial mechanisms of action have yet to be disclosed in the literature. However, the small size of the peptide may enable its permeation through the bacterium membrane. Another possibility, considering the similarities in MIC/MBC and the large associated concentrations, may be related with the encirclement

and isolation of the bacterial cells, with many peptide molecules acting against one bacterium cell, or with the blocking of specific regions along the cell membrane this way preventing exchange of nutrients and other viability-related factors, ultimately leading to the bacterium death [20]. Regardless, the obtained concentrations were considered elevated for fiber incorporation (not economically viable), which precluded the use of AAPV for its antibacterial effectiveness.

Despite its antimicrobial limitations, AAPV is known for its capacity to inhibit the activity of HNE, an enzyme which levels reach abnormally high ranks during inflammatory processes in CW [19]. Because of that HNE-related inhibitory profile, AAPV is still labelled an AMP [19]. In the case of inflammation, active HNE stimulates keratinocyte hyperproliferation, which can be balanced by low molecular weight peptide inhibitors, including AAPV [20]. Hydrophobic sequences of the peptide resemble amino acid regions of elastin, which are susceptible to HNE activity; hence, leading to the binding of the peptide to HNE subsites and resulting in a competitive HNE inhibition [17] The ability of AAPV to inhibit the HNE activity in CW-mimicking scenarios was examined using AAPV concentrations ranging from 0.100 to 200.000 μg/mL. Data reported a HNE maximum inhibitory concentration (IC_M) for the AAPV at 50 μg/mL, (Table S1 in Supporting Information). HNE inhibitory effect decreased at AAPV concentrations above the IC_M (<10 %). The same observation was reported in a study conducted by Namjoshi et al., in which HNE ability to digest the substrate decreased at the presence of larger concentrations of inhibitors [21]. Plausible explanations for such occurrence can be either related to the competition between the several peptide molecules present in solution or to the formation of agglomerates, thus reducing the availability of the peptide molecules for binding to the enzyme sites. On the other hand, HNE inhibition became more effective with increasing AAPV concentrations from 0.100 μg/mL up to IC_M. In fact, HNE inhibition did not vary significantly with AAPV concentrations above 3.130 μg/mL. These results may be explained by a potential equilibrium reached between the number of peptide molecules and the enzyme sites available for binding. This hypothesis gains strength when analyzing the results obtained with AAPV concentrations below 3.130 μg/mL; here, HNE inhibition was significantly reduced, most likely because of the insufficient amount of AAPV molecules available for binding to the enzyme activity-blocking sites. Although further research has been conducted towards the coupling of lipidic amino acids to AAPV towards an improvement of the peptide permeability across the *stratum corneum*, such peptide modifications still display lower HNE inhibitory effects than the native AAPV peptide [19,21]. To prevent the limitations associated with higher AAPV concentrations on HNE inhibition, the peptide was loaded onto the engineered co-axial fibers at the determined IC_M value. Even though AAPV at IC_M only guaranteed ≈16.5 % HNE activity inhibition, such effect was already deemed satisfactory since this enzyme intervenes as well in regenerative processes, working as a protecting wound agent against pathogens as it is released by neutrophils [16].

3.2. NCMC synthesis and characterization

CS has gained considerate attention towards wound healing applications. In fact, reports have proven the ability of CS to promote surface-induced thrombosis and blood coagulation, to accelerate tissue repair and to instigate tissue granulation, aside from protecting the wound from bacterial infections [22]. However, CS presents low solubility at pH above 6.5. Many approaches to synthesize CS derivatives have been addressed. Song et al. proposed a methodology for the selective alkylation of CS by means of pH and temperature control, which can lead to higher reactivity of NH_2 groups [12]. By reacting CS with chloroacetic acid in a neutral aqueous solution and by using 20 % w/v Na_2CO_3 as an acid binding agent, carboxymethyl groups can be introduced in free amine groups of CS, giving rise to NCMC. NCMC has been considered a promising derivative of CS for wound healing, by presenting excellent biocompatibility, biodegradability, low toxicity and effective antimicrobial activity [23].

NCMC was synthesized based on the protocol described by Song et al. with a yield of ≈71.5 %, which was influenced by variations in temperature and pH during the reaction and mass losses throughout the successive filtrations and centrifugations required for removal of unreacted CS [12]. Optimal reaction conditions were established at 90 °C for temperature, 4 h for reaction time and a mass ratio of chloroacetic acid/CS of 5/1. Low Mw CS (100–300 kDa) was used for the synthesis of NCMC, since both medium and high Mw did not perform as effectively (complete dissolution of CS was not accomplished). One explanation for such occurrence relies on the viscosity of CS which is directly proportional to its Mw, thus limiting the dissolution in the water/chloroacetic acid medium [24].

ATR-FTIR spectra of CS and NCMC were collected and compared for confirming the successful chemical modification of the polymer (Fig. 1a). Peaks at 1668, 1597 and 1404 cm^{-1} were detected in CS spectra, being assigned to amides I, II and III absorption bands, respectively [25]. Whereas, in NCMC spectra, two strong peaks were observed at 1590 and 1404 cm^{-1}, attributed to asymmetrical and symmetrical COO$^-$ groups stretching vibrations. CS's characteristic peaks at 1597 and 1668 cm^{-1} were replaced by a peak at 1590 cm^{-1} in NCMC spectra, indicating that carboxymethylation occurred on the free amine group of CS. In addition, the peak at 1032 cm^{-1} of CS, related to OH groups, remained unchanged, revealing that carboxymethylation did not occur in the OH groups of CS. NMR spectrum of NCMC (Fig. 1b) reported signals in the range of 4.40–5.00 ppm, which were related to hydrogen bonded to the carbon atom C1. Whereas the signal centered at 2.90–3.10 ppm referred to hydrogen bonded to the carbon atom C2 of the glucosamine ring. In addition, signals centered in the range 3.30–4.00 ppm corresponded to hydrogen atoms bonded to carbon atoms C3, C4, C5 and C6 of the glucopyranose. NMR data attested to the successful synthesis of NCMC, which was also consistent with [12]. Additionally, the DS of amine groups into carboxymethyl groups was determined at ≈0.98. According to Ge et al., a substitution of CS into NCMC can be deemed successful when DS is superior to 0.85 [13].

NCMC showed bacterial inhibition towards the Gram-positive bacterium *S. aureus*. MIC of NCMC against *S. aureus* was found at 1.536 mg/mL, with MBC being established at 3.072 mg/mL. Several reports in literature have confirmed the antibacterial activity of CS derivatives, including NCMC [12,13,23]. Nevertheless, the mode of action of CS derivatives is still not fully understood. According to Wen et al., one possible mechanism is related to alterations in cell permeability caused by electrostatic interactions between the positive CS backbone and negatively charged cell surface. Such interactions can also result in the leakage of intracellular constituents, leading to cell death [23]. Another possibility relies on the penetration of CS through the plasma membrane, binding with the nucleic acid and affecting the DNA expression of the bacterial cell, compromising its replication abilities and other biological functions highly important for the bacterium survival [26]. Since the substitution of amine groups by carboxymethyl groups is not complete, it is possible that NCMC may present a somewhat similar antimicrobial profile to CS. Considering, *S. aureus* has been reported as one of the most prevalent bacteria present in CW, NCMC was loaded into the fibers at 2xMBC [27]. This loading concentration was selected based on previous works conducted by our team in which the incorporation of antimicrobial agents into polymer constructs led to a reduction of the agents' antimicrobial activity. Such agents remained trapped in the polymeric matrices, establishing polymeric interactions and, therefore, losing reactive groups that otherwise would be available for interacting with the microorganisms [18].

3.3. Wet-spun fibers morphology

Viscosities of SA, SA-NCMC, PCL and PCL-AAPV solutions were determined at varying RT, to resemble fibers production conditions (Fig. S2 in Supporting Information). Results confirmed that viscosities of
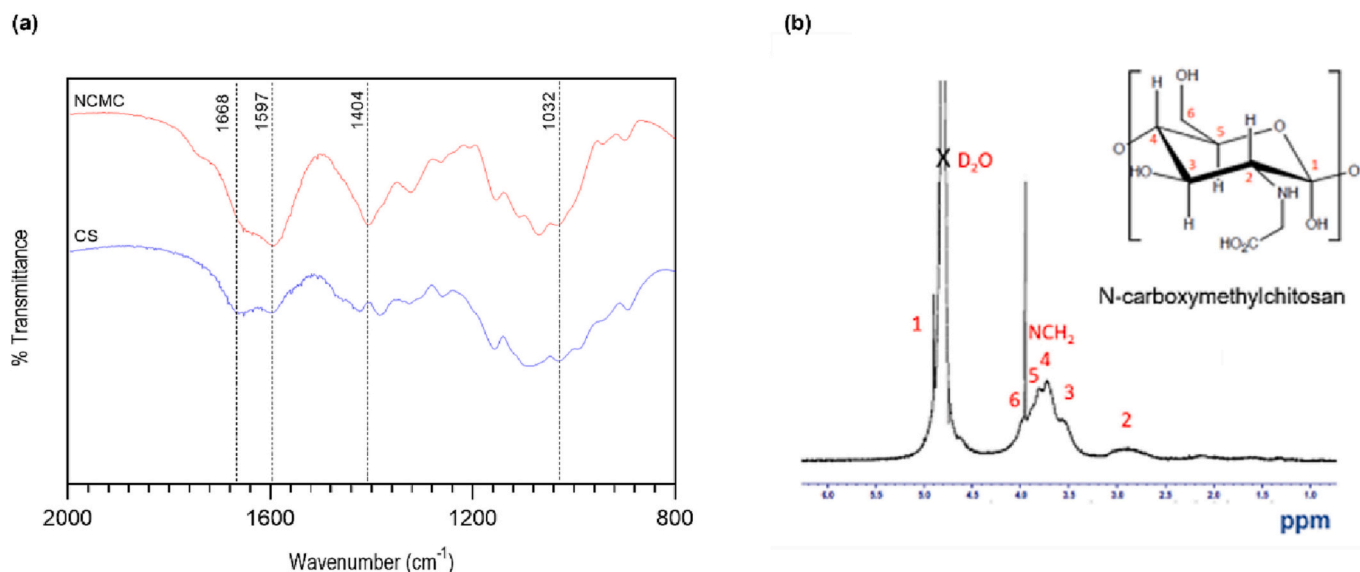
Fig. 1. (a) ATR-FTIR spectra of CS and NCMC (2000–800 cm^{-1}), and (b) ^{1}H NMR spectra of NCMC in D$_2$O.

SA and SA-NCMC solutions were inversely proportional to temperature, as it has already been addressed in many reports [28]. Moreover, it was evident that the SA solution was more viscous than the PCL solution, which explains the small fluctuations registered in shell thickness during co-axial fiber production (Fig. 2c). The addition of NCMC to SA decreased the solution's viscosity (Fig. S2 in Supporting Information).
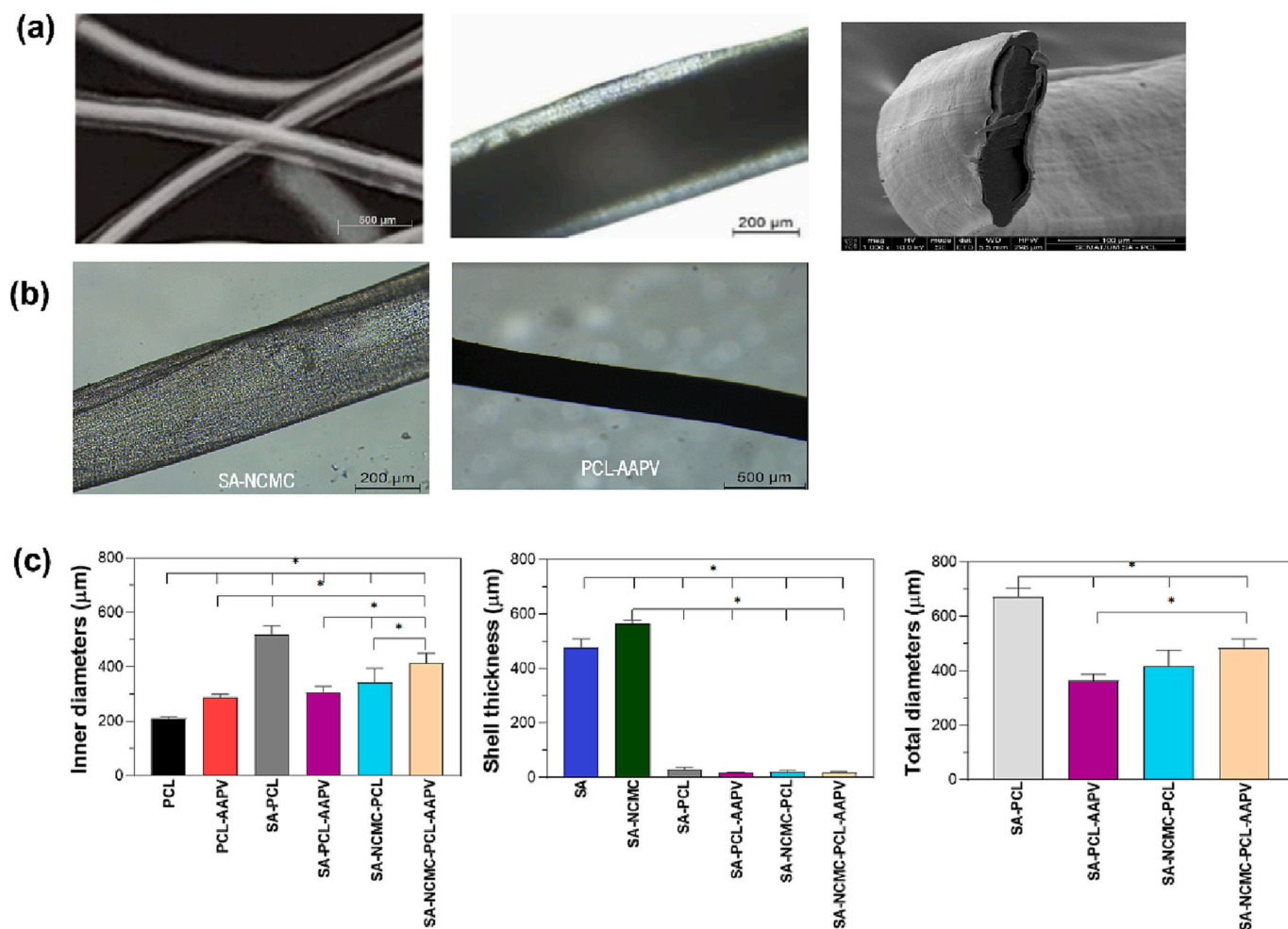

Fig. 2. (a) Micrographs of SA-NCMC-PCL-AAPV wet-spun fibers morphology, obtained by brightfield and SEM microscopy. (b) Micrographs of PCL-AAPV and SA-NCMC wet-sun fibers obtained by brightfield microscopy. (c) Distribution of fiber diameters and thicknesses. Data are reported as mean ± SD (n = 5). Statistical significance was determined via Tukey test applying multiple comparisons between the different fiber typologies (*p < 0.001).

Such observation can be justified with the low viscosity inherent to CS-derivatives [24], the use of a low Mw polymer for NCMC synthesis, or with the possible interruptions NCMC introduced in the polymeric chains of SA via chemical bonding, generating more easily breakable sites and thus altering the rheological properties of the solution. That same effect was observed with the addition of AAPV to the PCL solution; the low Mw of AAPV also translates into a lower viscosity [19]. Nevertheless, as AAPV was incorporated into the PCL solution at a lower concentration than NCMC, the reduction in viscosity faced by PCL was less pronounced than that endured by SA.

SEM micrographs of the fibers' cross-section are shown in Fig. 2a, also confirming the formation of co-axial structures. Fibers' thicknesses were measured using Image J® software. Residual fluctuations of thicknesses between the same fiber typology were observed. As shown earlier, these were expected because of differences in polymer viscosity with temperature variations (Fig. S2 in Supporting Information). Regarding the hollow and monolayered fibers, it was seen that the addition of NCMC and AAPV to SA and PCL, respectively, led to an increase in the fibers' thickness. Such observations can be justified by the alterations of each of the additive components introduced in the polymeric chains (binding can be done through the main and the side chains), resulting in less compact structures [18]. Additionally, the decrease in solutions' viscosities, which confirmed the loading of such components, significantly altered the solutions' rheological properties and thus their ejection towards the coagulation bath. PCL and PCL-AAPV fibers presented smaller thicknesses than the SA and SA-NCMC hollow fibers. Because of their hollow interior, SA-NCMC fibers tended to collapse as they were being collected. As a result, flattened structures with visible folds were formed, justifying the larger thicknesses detected (Fig. 2b).

Regarding the co-axial fibers, it was observed that the shell's thickness was significantly inferior to the core, possibly due to interactions between PCL and SA. To confirm that theory, a small amount of PCL solution was put in contact with SA solution (Fig. S3 in Supporting Information). After a few seconds, PCL quickly precipitated in the presence of the SA solvent (dH_2O) and grew in volume (without altering the total volume of the combined solutions), which shows that the PCL matrix incorporated part of the SA, thus explaining the increase in thickness of the core components compared to the monolayer testing [29]. It is likely that the OH groups content of each polymer to facilitate bond formation [30]. Similar observations were made by Dodero et al. when producing a multilayer membrane via electrospinning composed of SA and PCL [31]. Although there are several reports on SA and PCL composites, to the authors' knowledge their chemical interactions are still not fully explained.

Additionally, the presence of NCMC and AAPV at the shell and core of the fibers, respectively, caused further reduction of the shell thickness. These bioactive additives led to changes in the conformation and organization of both SA and PCL polymeric chains, generating more interactions between fiber components at different locations (core and shell). Furthermore, contrary to the monolayer fibers (PCL-AAPV and SA-NCMC) where side chains had more freedom, here they were restricted by the presence of another layer, reducing fiber dilatation [18].

3.4. ATR-FTIR of the engineered wet-spun fibers

ATR-FTIR spectra were collected for all engineered fibers (Fig. 3) and characteristic peaks were identified (Table S2 in Supporting Information). In SA-containing fibers (Fig. 3a and c), two visible bands at 1600 and 1420 cm^{-1}, being related to COO^- vibrations, along with a band at 3300 cm^{-1} characteristic of OH groups, confirmed the presence of this polymer [18]. On its turn, presence of PCL was verified in all PCL-containing fibers by characteristic peaks at 1725 cm^{-1}, related to C=O stretching vibrations, which was less pronounced on co-axial fibers since PCL was present in the innermost layer of the fiber
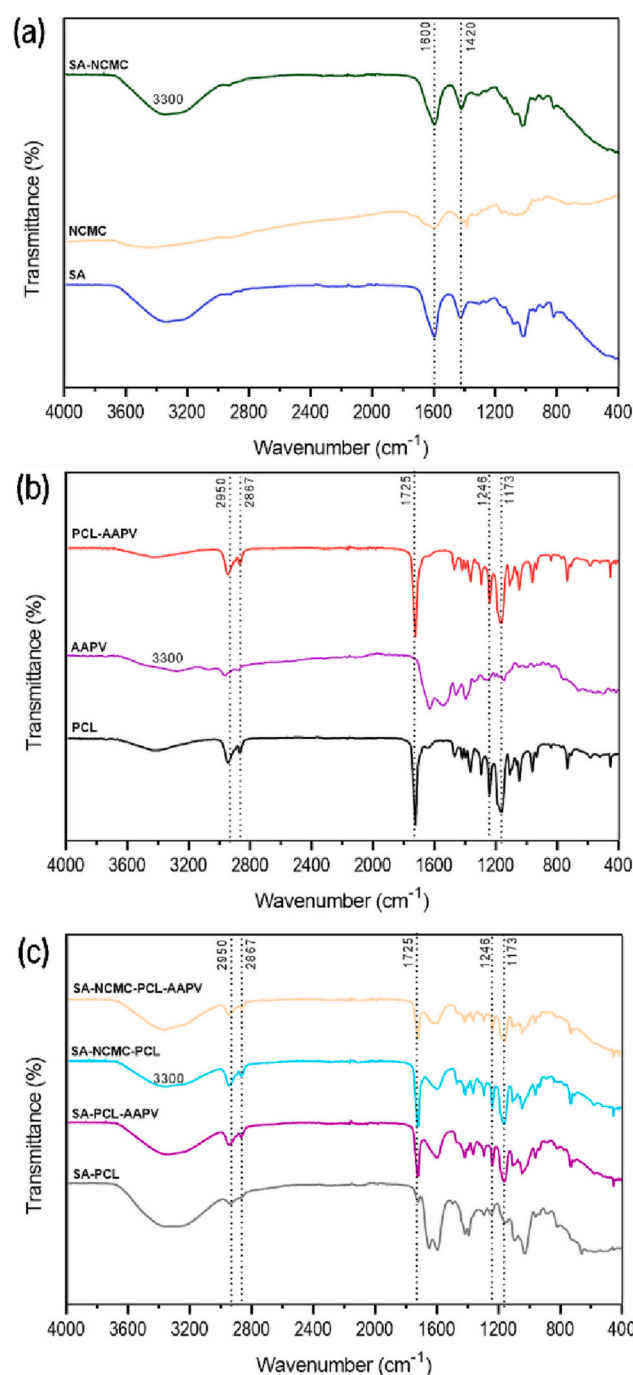

Fig. 3. ATR-FTIR spectra of (a) SA, NCMC and SA-NCMC fibers, (b) PCL, AAPV and PCL-AAPV fibers, and (c) the co-axial wet-spun fibers.

conditioning its detection [32]. Moreover, bands at 2867 and 2950 cm^{-1} associated with CH stretching vibrations also confirmed the presence of this polymer, together with bands at 1173 and 1246 cm^{-1} referring to C—O—C vibrations [33]. Considering NCMC and AAPV were loaded at small concentrations, it was not possible to confirm their presence in the co-axial fibers via ATR-FTIR, even though viscosity alterations imposed by these additives had been previously observed confirming their presence and influence in the base polymers (Fig. S2 in Supporting Information).

3.5. Thermal characterization

DSC thermograms were collected for all fibers to assess their thermal

behavior (Fig. 4 and Table S3 in Supporting Information). Two main SA characteristic peaks were observed on SA-containing fibers, one broad endothermic peak centered at ≈138 °C (onset at 86 °C) and a higher endothermic peak centered at ≈235 °C (on set at 167 °C). The first was related to the loss of water molecules from SA, whereas the second resulted from the polymer thermal decomposition, associated with degradation, dehydration and depolymerization reactions from the carboxylic groups of SA [18]. The addition of NCMC to the fibers resulted in the introduction of an endothermic peak centered at ≈176 °C (on set at 165 °C) linked to NCMC melting and evaporation of water molecules present in the sample [34]. Moreover, an overlap of broad exothermic peaks occurred at ≈219 °C (on set at 184 °C). This can be associated with the degradation and depolymerization reactions of carboxylic groups of both SA and NCMC, along with polysaccharide ring dehydration and decomposition of acetylated CS [18]. Literature reports address these same thermal events at higher temperatures (≈270 °C) for carboxymethyl chitosan (CMC). It is likely that such shifts in temperatures detected for NCMC to result from the interactions established with SA. Furthermore, no glass transition temperature (T_g) was registered, indicating the amorphous nature of NCMC [34].

PCL-containing fibers presented an endothermic peak centered at ≈59 °C (onset at 56 °C) referring to the first melting temperature of PCL and the fusion of its short polymer segments. A second melting temperature was also registered with an endothermic peak at ≈133 °C (onset at 123 °C). Moreover, degradation of the polymer segments initiated at ≈200 °C, which was consistent with previous reports [35]. The incorporation of AAPV onto the fibers did not induce any visible/significant alterations on the thermograms since the peptide was loaded at a very low concentration (50 μg/mL). As expected, PCL characteristic peaks were less pronounced on co-axial fibers because of the influence of the shell components (SA and NCMC) [36]. Such observation was also consistent with ATR-FTIR data (Fig. 3). Still, even though less pronounced, the main thermal events characteristic of both SA and PCL polymers were observed on all co-axial structures, with similar onset temperatures, in comparison with monolayer and hollow fibers. Most importantly, the presence of NCMC was corroborated.

3.6. Mechanical testing

Maximum elongations at break of wet-spun PCL-containing fibers were analyzed using 10 cm long filaments. Such tests were carried out with the purpose of evaluating the fibers' mechanical resistance. SA and SA-NCMC hollow fibers could not be examined since after wet-spinning collection they became flattened, with many easily breakable sites along with many visual folds, resultant from fiber collapse towards the hollow interior. Reports have addressed the poor mechanical properties of SA on its own as an obstacle for several applications [37]. Nevertheless, that does not significantly influence fibers ejection, since the final application depends on the properties of all fiber compounds working together.

In general, high elastic capacities (maximum elongations at break superior to 133 %) were obtained for the remainder fiber typologies (Fig. 5), due to the inherent elasticity of PCL [38]. In the monolayered fibers, it was noticeable that the addition of AAPV slightly decreased fibers' elongation, since the proportion of the elastic component (PCL) was reduced. As seen earlier, AAPV decreased the viscosity of PCL and altered its chains' organization/structure, introducing weaker links (Fig. S2 in Supporting Information).

Results showed that co-axial fibers presented higher maximum elongations and better mechanical performances than PCL and PCL-AAPV monolayered fibers (Fig. 5 and Table S4 in Supporting Information). This is justified with the presence of the shell that offered protection and delayed the rupture of the core (Fig. S in Supporting Information). Additionally, the thickness of the core was higher in the co-axial fibers than monolayered fibers, due to the partial incorporation of SA present in the shell (Fig. S3 in Supporting Information). Several reports attest to these data, showing that higher mechanical properties

are attained by PCL-based co-axial fibrous structures compared to monolayered constructs [39].

The addition of NCMC led to a decrease in the fibers' elongations, which was also expected considering its effect in the SA solution's rheological behavior, along with the potential alterations and chain interruptions NCMC introduced in the conformation and structure of the SA (presence of weaker structural sites by NCMC binding). In fact, several reports have been published, addressing NCMC as a CS-derived polymer with poor mechanical properties [40]. As a result, SA-PCL co-axial fibers presented the highest maximum elongations, since they did not include AAPV nor NCMC in their composition, and thus fibers' elasticity was not compromised by these additives. By comparing SA-NCMC-PCL with SA-PCL-AAPV fibers, it was possible to conclude that the incorporation of AAPV had a smaller influence in the fibers' elasticity than NCMC, an expected outcome considering the loading amounts. Therefore, from the co-axial fiber group, SA-NCMC-PCL-AAPV fibers displayed the lowest maximum elongations; yet, still within acceptable ranges for the foreseen application.

3.7. Swelling capacity

The degree of swelling of the produced wet-spun fibers was determined by measuring mass alterations after incubating the materials in PBS at 37 °C until saturation was reached (24 h). Testing was conducted in PBS solution because of its resemblance with the osmolarity and ion concentration of human biological fluids [10]. Samples were weighted after different periods of incubation so the moment at which equilibrium was reached could be detected. At 24 h of incubation variations in mass were no longer detected, so swelling ratios could be determined (Table 1).

SA and SA-NCMC hollow fibers reported the highest swelling degrees, namely 836.38 ± 115.60 and 1337.90 ± 86.82 %, respectively, confirming the affinity of SA towards water. Many studies on SA-containing fibers and hydrogels have addressed the excellent hydration properties and swelling capacities of SA, with swelling occurring instantly in contact with PBS and achieving values up to ≈476 % [11]. Here, the degree of swelling was even superior, most likely a result of the large surface area of the fibers (inner and outer surface exposed to medium). According to Bajpai et al., this can also be related to the presence of residual Ca^{2+} from the coagulation bath that, when in contact with PBS, undergo ion-exchange processes with Na^+ ions, also binding with COO— groups from SA. Electrostatic repulsions between negatively charged COO— groups take place, causing chain relaxation and resulting in higher swelling degrees. The ion-exchange process may also be responsible for generating a looser structure, as phosphate ions from PBS interact with Ca^{2+}, forming calcium phosphate and, therefore, raising the water intake of the fibers [41]. Loading NCMC onto the SA hollow fibers increased almost 1.6-fold their swelling degree. NCMC also displays excellent water-retention ability and affinity [12]. NCMC presents a similar molecular structure to alginate, in reference to the carboxyl groups, therefore leading to an excellent miscibility and compatibility between SA and NCMC, made of intermolecular bonds (i. e., hydrogen). Such observations are in accordance with research conducted by Fan et al., in which blends of alginate and CMC showed improvements in water-retention capacity over the pure alginate fibers (398 % vs 91 %) [42]. Additionally, considering the alterations introduced by NCMC on the SA polymeric chains, as seen by the increment in shell thickness (Fig. 2), it is also possible that new conformation arrangements and polymer chain expansion to have increased the fiber surface area and, with that, allowed for more free OH— groups to become exposed and available for interactions with PBS water molecules.

PCL and PCL-AAPV fibers presented the lowest degrees of swelling (49.20 ± 18.19 and 54.25 ± 9.06 %, respectively), reflecting the hydrophobic character of PCL, which limits the interactions with water molecules via polymer repulsion [87,88]. Such observation is coherent
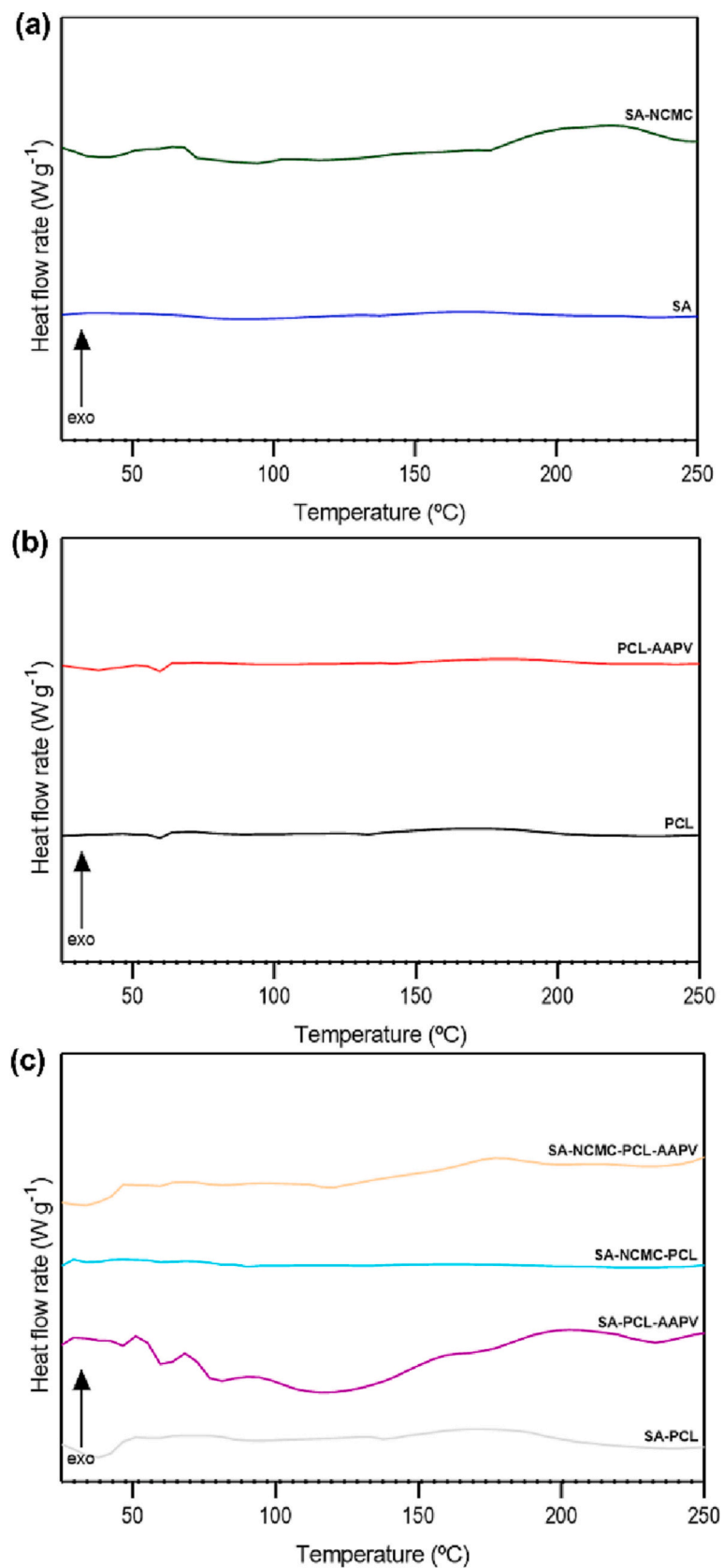
Fig. 4. DSC thermograms of (a) SA and SA-NCMC hollow fibers, (b) PCL and PCL-AAPV fibers, and (c) co-axial wet-spun structures.
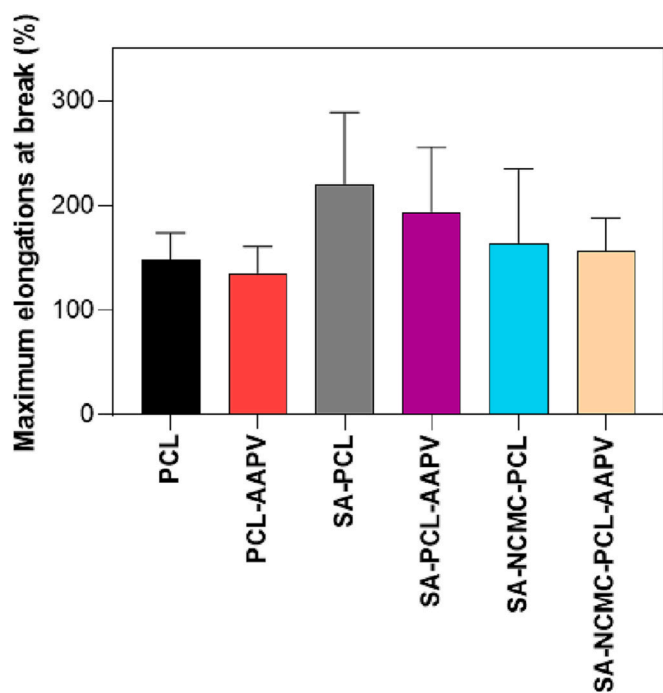
Fig. 5. Maximum elongations at break attained for each fiber typology. Data are reported as mean ± SD (n = 4).

with a report from Lee et al., in which the addition of PCL onto SA beads limited the degree of swelling because of the length of the hydrophobic PCL chains [43]. AAPV addition slightly improved the PCL fibers swelling behavior, as AAPV possesses many hydrophilic groups [89]. Additionally, as previously addressed, the incorporation of AAPV into the PCL solution altered its rheological behavior and, with that, possibly the conformation and structural arrangement of the polymer chains. Such improvement in degree of swelling upon addition of AAPV and NCMC was also noticeable on the SA-PCL-AAPV (277.27 ± 5.96 %), SA-NCMC-PCL (283.40 ± 26.27 %) and SA-NCMC-PCL-AAPV (324.36 ± 68.94 %) fibers. In fact, SA-PCL displayed the lowest swelling ratios amongst the co-axial fibers (172.82 ± 13.24 %). This happened because PCL was present at a greater polymer proportion, even partially incorporating SA at the fibers' core and, thus, blocking its ability to absorb water, and exposing more hydrophobic groups, limiting wettability. Furthermore, SA-NCMC-PCL-AAPV fibers presented higher degrees of swelling in relation to SA-PCL-AAPV and SA-NCMC-PCL fibers, possibly due to the presence of two hydrophilic additives (AAPV and NCMC).
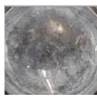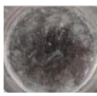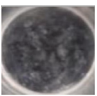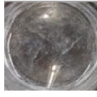
3.8. Degradation profile
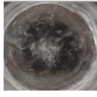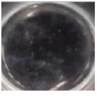
The stability of unloaded and NCMC- and AAPV-loaded wet-spun fibers in PBS was evaluated up to 28 days of incubation at 37 °C. Once again, PBS adjusted to pH 7.4 was selected to approximate testing conditions to physiological environments, to which NCMC is responsive [44].

Fibers' degradation was assessed visually and by tracking mass alterations over time (Table 1). Data revealed that SA and SA-NCMC hollow fibers were the least stable fibers. After 14 days of incubation in PBS, hollow fibers suffered high mass losses and it was no longer possible to determine their weight. Such observations were expected due to the absence of PCL, which main function was to maintain the fibers' structural integrity for longer periods of time, and to the hollow interior of the fibers, which conditioned the mechanical resilience of the structures (Fig. 5) and flattened the fibers, evidencing many folds (Fig. 2b). In fact, several studies on the degradation of SA fibers immersed in PBS have reported a fast degradation, mainly caused by the hydrolysis of β-1,4 glycoside bonds present in alginate molecules [45]. Similar observations were also addressed in a research by Homem et al., in which SA fibers were highly hydrated, resulting in the loss of their structural forms and causing the formation of agglomerates after 7 days of incubation in simulated body fluid [18]. As expected, the addition of NCMC led to higher mass losses, since NCMC also presents hydrophilic properties and, as previously referred, establishes interactions via intermolecular hydrogen bonds with SA, interrupting the polymer chain and altering its structural conformation (Fig. 5). Such results are also in accordance with several studies on the degradation of SA and CMC blend structures on PBS, in which the incorporation of CMC increased degradation, compared to SA pure structures [18]. On the other hand, PCL-containing fibers kept their structural integrity throughout the 28 days of incubation. Similar outcomes have been reported, showing, for instance, that the incorporation of PCL onto polymer composite fibers can diminish the overall degradation profile of the scaffolding system when incubated in PBS [46].

Interestingly, PCL and PCL-AAPV fibers registered mass increments, most likely caused by bonds generated between PCL and salts from PBS. According to Shamsah et al. and Huang et al., the carbonyl group of PBS presents high nucleophilicity, caused by the polarity of an ester group. As a result, strong hydrogen bonds are formed between the carbonyl group of PBS and the methylene group of PCL [46]. On the other hand, co-axial fibers suffered from the fast shell degradation effect introduced by SA and/or NCMC, while also experiencing the binding of PCL with PBS salts. Data demonstrated that the effect of shell degradation overlapped PBS salts binding to PCL, with all co-axial fibers undergoing mass loss throughout the 28 days of incubation. This is in agreement with several studies exploring the production of SA and PCL structures, in

Table 1

Wet-spun fibers degradation profiles over 28 days of incubation in PBS. Data are presented as average percentage of mass loss ± SD (n = 3).

Fiber	Mass loss (%)					
	Day 1	Day 3	Day 7	Day 14	Day 21	Day 28
SA	1.30 ± 0.52	11.18 ± 3.99	74.37 ± 0.79			
SA-NCMC	5.62 ± 2.79	12.23 ± 7.08	81.43 ± 1.97			
PCL	−4.27 ± 11.36	−6.78 ± 2.26	−6.22 ± 7.19	−10.66 ± 13.99	−13.94 ± 10.81	−30.67 ± 19.90
PCL-AAPV	−6.10 ± 28.12	−8.64 ± 3.01	−7.85 ± 15.75	−20.64 ± 1.33	−14.48 ± 2.06	−33.78 ± 12.58
SA-PCL	14.87 ± 5.85	12.42 ± 1.81	11.44 ± 4.55	16.41 ± 1.24	2.71 ± 1.05	3.46 ± 1.94
SA-PCL-AAPV	16.64 ± 9.01	16.65 ± 10.53	13.80 ± 12.34	21.59 ± 1.13	2.85 ± 1.77	6.11 ± 1.83
SA-NCMC-PCL	18.08 ± 3.69	20.96 ± 5.73	14.08 ± 3.24	22.91 ± 8.66	3.38 ± 2.87	6.07 ± 1.84
SA-NCMC-PCL-AAPV	20.37 ± 10.56	23.16 ± 11.76	16.17 ± 14.35	25.34 ± 5.55	4.36 ± 3.42	6.84 ± 4.07

which the SA layers' fast degradation profile compromised the structural integrity of the entire material [37].

Between all co-axial fibers, SA-PCL was the ones that registered the lowest mass losses, due to the absence of AAPV and NCMC. The addition of AAPV to the core increased bonds with water molecules since AAPV presents a hydrophilic character, whereas the incorporation of NCMC altered the conformation of SA polymeric chains, forming intermolecular hydrogen bonds [42]. Therefore, SA-NCMC-PCL-AAPV presented higher degradation rates in comparison with SA-NCMC-PCL and SA-PCL-AAPV fibers, due to the presence of both AAPV and NCMC (superior hydrophilic characters), which is in line with the results obtained in the swelling behavior experiments (Section 3.7).

3.9. AAPV release kinetics

The AAPV's release kinetics from the wet-spun fibers was followed by loading fibers with Fmoc-AAPV (yield 78 %), a modified version of AAPV in which a Fmoc group remained attached to the N-terminal alanine (characterization in Section S3 in Supporting Information). Such modification endowed the peptide with fluorescence, which allowed the detection of the release of AAPV in a selective manner by fluorimetry, no longer overlapping with the detection of the remaining fiber compounds by absorption spectroscopy. It should be noticed that the presence of the Fmoc group did not alter the mechanical and physical properties of the fibers. Data was collected after 1, 2, 4, 6 and 24 h of incubation in PBS at 37 °C (Fig. 6).

The absence of a shell in the PCL-AAPV fibers resulted in a quick burst release of the peptide during the first hour of incubation ($\approx$16.94 %). After this period, release was done at a slower pace, considering less amount of peptide was available along the fibers. From all tested substrates, PCL-AAPV registered the highest release profiles. These observations were expected considering the main function of the shell is to act as a protective barrier, controlling the release of the encased bioactive agents, and here such protection was absent [9].

On the other hand, SA-PCL-AAPV and SA-NCMC-PCL-AAPV fibers showed similar release profiles, being more prolonged in comparison with PCL-AAPV fibers and achieving the maximum rate at the 6 h target (Fig. 6). SA-NCMC-PCL-AAPV fibers showed a slightly higher release profile than SA-PCL-AAPV fibers because of the presence of NCMC, which is responsive to the pH of the medium (physiological) [44]. As previously addressed, the incorporation of NCMC onto the shell led to the formation of interactions via hydrogen bonds with SA, causing a faster shell degradation in comparison with SA-PCL-AAPV fibers (Table 1). As shell degradation occurred, its protective effect decreased,

therefore allowing for a greater release of AAPV from the fibers' core and, thus, explaining the higher release rates observed for the SA-NCMC-PCL-AAPV samples.

3.10. HNE inhibition via AAPV-loaded fibers

HNE activity was followed for 1, 2, 4, 6 and 24 h in PBS at 37 °C in contact with AAPV-loaded fibers to assess their ability in inhibiting the enzyme performance and, once again, confirm AAPV incorporation (Fig. 7). Data from fibers free from AAPV was also collected so the polymers' interference could be eliminated from the results.

In the first hour of incubation, an initial burst release of AAPV was detected (Fig. 5), explaining the elevated HNE inhibition ($\approx$17.11 % for PCL-AAPV, $\approx$18.33 % for SA-PCL-AAPV and $\approx$19.18 % for SA-NCMC-PCL-AAPV fibers). Consequently, as more AAPV was released from the fibers' surface in the first instances of contact, less AAPV was available at the 2 h mark, explaining the decrease in HNE inhibition. Yet, after 2 h
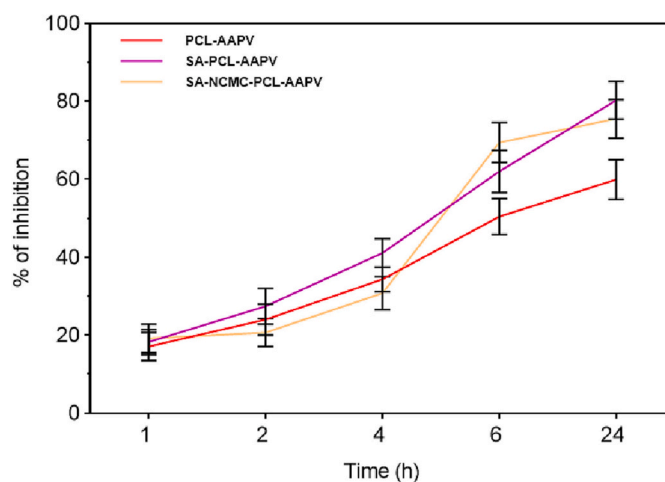
Fig. 7. HNE inhibition profile induced by AAPV-loaded wet-spun fibers. Data are reported as mean ± SD (n = 9). Statistical significance was determined via Tukey, applying multiple comparisons between the different fiber typologies (significance between PCL-AAPV and SA-PCL-AAPV: $p < 0.006$ at 4 h, no significance was found at 1, 2, 6 and 24 h; significance between PCL-AAPV and SA-NCMC-PCL-AAPV: no significance was found; significance between SA-PCL-AAPV and SA-NCMC-PCL-AAPV: $p < 0.006$ at 2 h, $p < 0.0001$ at 4 h, no significance was found at 1, 6 and 24 h).
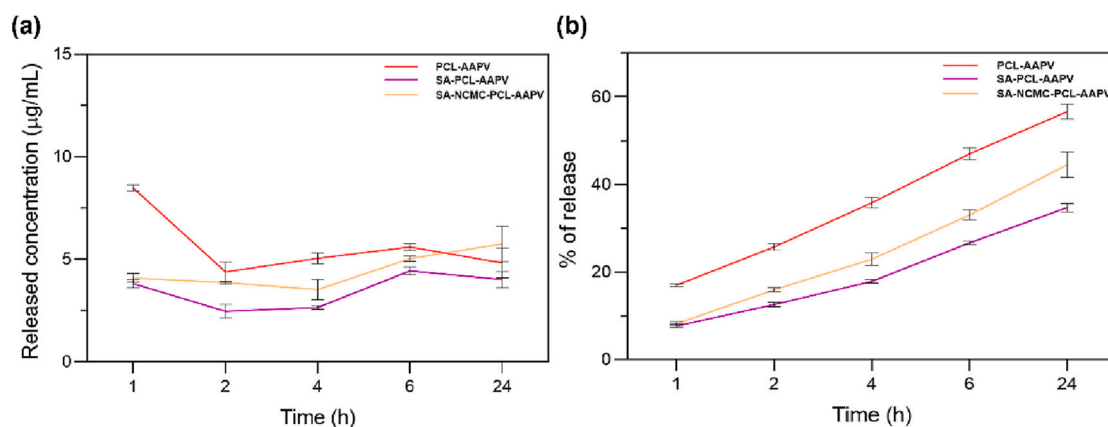
Fig. 6. Release profile of AAPV-loaded wet-spun fibers expressed in (a) concentration of peptide release at each time period (μg/mL) and (b) cumulative % of peptide released. Data are reported as mean ± SD (n = 3). Statistical significance was determined via Tukey test, applying multiple comparisons between the different fiber typologies (significance between PCL-AAPV and SA-PCL-AAPV: $p < 0.0001$ at 1, 2, 4, 6 and 24 h; significance between PCL-AAPV and SANCMC-PCL-AAPV: $p < 0.0001$ at 1, 2, 4 and 6 h, $p < 0.0020$ at 24 h; significance between SA-PCL-AAPV and SA-NCMC-PCL-AAPV: $p < 0.0040$ at 2, 4 and 24 h, $p < 0.0020$ at 6 h, no significance was found at 1 h).

of incubation in PBS, the efficacy of the AAPV-loaded fibers against HNE increased. As time passes and as the fibers absorb and desorb molecules from the surrounding medium, the AAPV loaded at the fibers' core can migrate to the surface, thus enabling more peptide molecules to be released and to become available to act against HNE. It is also likely that, due to the interactions between PCL and PBS (Table 1), the PBS salts to have blocked momentarily the release of AAPV from the fibers' core, conditioning its inhibitory effect. At the 6 h mark, the highest percentages of HNE inhibition were observed for all fibers, which is consistent with the highest release rate of AAPV (Fig. 6). After this point, as AAPV was at a smaller amount in the fibers, smaller inhibitory effects were detected against the enzyme.

PCL-AAPV displayed lower HNE inhibitory profiles in comparison with the AAPV-loaded co-axial fibers, possibly due to the affinity of PCL towards PBS salts (Table 1), which could have limited the availability of AAPV. SA-PCL-AAPV and SA-NCMC-PCL-AAPV fibers presented similar HNE inhibition during the first 6 h of incubation in PBS. However, at the 6 h mark, HNE inhibition became more important on the NCMC-containing fibers. Although there are no reports addressing the NCMC effect on the HNE activity, Chopra et al. demonstrated that CS can inhibit elastase activity [47]. Since the modification of CS into NCMC did not occur in all amine groups, it is possible that this inhibitory effect may be present as well in NCMC, thus explaining the higher HNE inhibition compared to the SA-PCL-AAPV fibers. Moreover, as previously observed, the presence of NCMC caused a faster shell degradation, in comparison with a shell of pure SA (Table 1). Therefore, it is also possible that this faster shell degradation to have resulted in more exposure to the AAPV molecules.

3.11. Bacteria inhibition

S. aureus growth inhibition induced by NCMC-loaded and unloaded fibers was examined after 1, 2, 4, 6 and 24 h of incubation at 37 °C. Results were expressed in log reduction and number of colonies forming units (Fig. 8 and Fig. S6 in Supporting Information, respectively). After 2 h of incubation, SA-NCMC hollow fibers presented the highest log reduction, possibly due to their flattened structure and fast shell

degradation (Table 1). Although it was not possible to map NCMC release kinetics in PBS, due to overlaps of maximum absorbances from many fiber compounds, it is expected NCMC to follow a similar release profile to AAPV, being even instigated by the pH of the surrounding media (7.4). It is likely that the SA-NCMC shell degradation caused the fast release of NCMC, becoming highly available to inhibit *S. aureus* activity. To the authors' knowledge, there are still no reports on the mode of action of NCMC. Nevertheless, it is known that CS derivatives develop molecular-level interactions with the cell membrane of bacteria [48]. In addition, several researches addressed that the damage of bacteria cell membranes is related to electrostatic, ionic, or hydrophobic interactions and that the density of the electric charges on the surface of the bacteria strongly influences the amount of CS or CS derivatives adsorbed, which alter the membrane's structure and permeability [48]. Furthermore, as previously discussed, NCMC also possesses hydrophilic characteristics, having reported high degrees of swelling, which enabled NCMC to establish strong interactions by hydrogen bonding with water molecules from PBS. It is also possible that, in parallel with those interactions, the breaking of pre-established SA-NCMC bonds might have occurred, therefore, releasing high amounts of NCMC and substituting it with water molecules. Nevertheless, the antibacterial effect from such fibers reduced after the 2 h mark, possibly due to the less amount of NCMC being available after this first interaction with the surrounding environment.

SA-NCMC-PCL and SA-NCMC-PCL-AAPV co-axial fibers presented lower log reduction, in comparison with SA-NCMC fibers. Since both fibers typologies displayed superior structural stability in PBS (Table 1), it is likely that the NCMC could be released in a more controlled and prolonged manner, explaining the smaller antibacterial effect compared to the hollow fibers. In fact, both co-axial fiber typologies presented similar log reduction values throughout the 24 h of incubation in PBS, achieving higher rates at the 6 h mark. However, SA-NCMC-PCL-AAPV still presented a slightly higher log reduction. One plausible explanation for that is associated with an interference caused by the presence of AAPV which, as previously disclosed, presented antibacterial activity against *S. aureus* (MIC/MBC of 2.048 mg/mL). Such hypothesis was also supported by the fact that PCL-AAPV and SA-PCL-AAPV presented
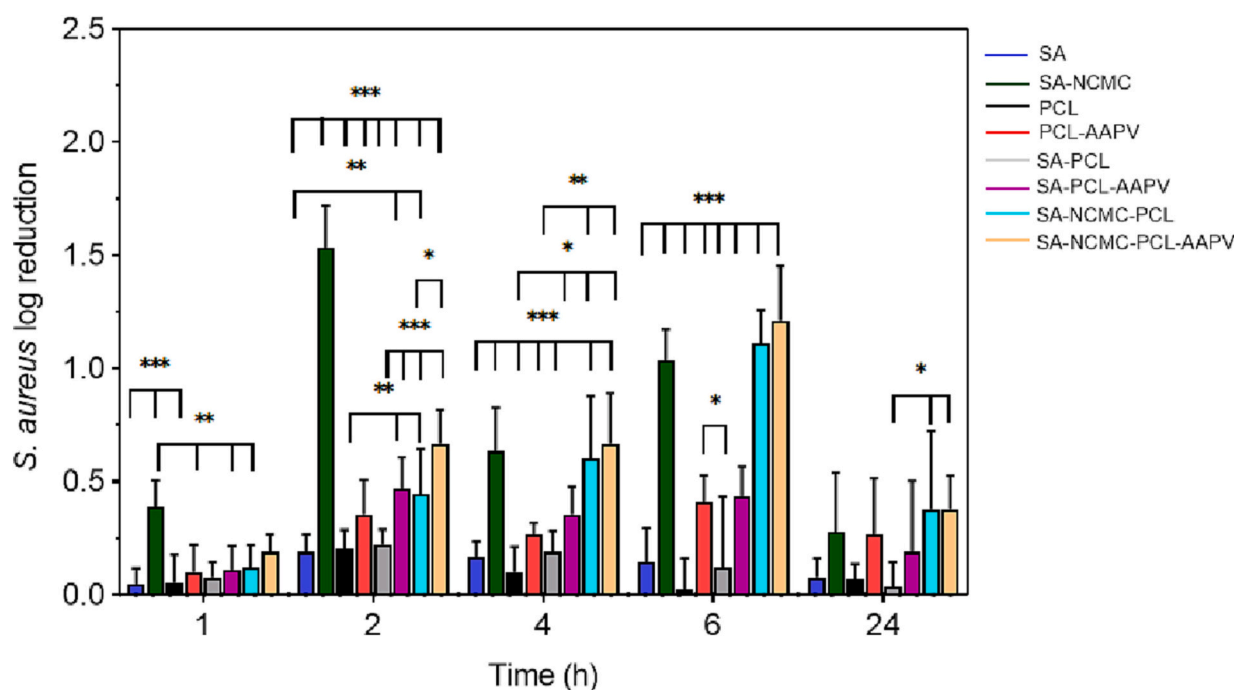

Fig. 8. *S. aureus* log reduction in contact with all wet-spun fibers incubated in PBS for 1, 2, 4, 6 and 24 h. Data are reported as mean ± SD (n = 3). Statistical significance was determined via Tukey test applying multiple comparisons between the different fiber typologies *p < 0.05; **p < 0.003; ***p < 0.0005.

higher log reductions in comparison with AAPV and NCMC unloaded fibers. Interestingly, both fiber typologies also induced superior bacteria inhibition at the 6 h mark, coinciding with the higher release of AAPV from the fibers (Fig. 6). In the future, additional work will be conducted on the AAPV antimicrobial profile and its potential synergisms with other bioactive agents, including NCMC. As expected, the bacteria viability tendency was for the number of dead colonies to increase with longer periods of incubation (Table S5 in Supporting Information). Yet, between 6 and 24 h testing, coinciding with a smaller impact of AAPV and NCMC, the live bacteria multiplied, making the fibers incapable of combatting their growth and stopping their proliferation, which is also evident by a smaller log reduction in Fig. 8.

AAPV and NCMC unloaded fibers still reported residual log reduction values which may be justified with the presence of remaining Ca^{2+} salts from the coagulation bath since calcium ions have been reported to possess antibacterial properties [49]. All in all, it was noticeable that NCMC-loaded fibers showed the highest log reduction against *S. aureus*, confirming the antibacterial properties of this CS derivative.

3.12. Cytocompatibility

Cytocompatibility examinations via cell metabolic activity and cell lysis assays were conducted by direct contact of all wet-spun fibers with L929 and HaCaT cell lines (Fig. 9). These cell lines were selected based on their predominance on the epidermis (keratinocytes) and connective tissue (fibroblasts), thus better approximating the testing conditions to real-life scenarios [50].

According to ISO standard 10,993–5:2009, a cytotoxic effect is defined by a reduction in cell viability (cell lysis) of >30 %. Such effect was detected on SA-NCMC fibers (cell lysis of ≈30.89 %) for L929 cell line and on SA, SA-PCL and SA-PCL-AAPV fibers for HaCaT cell line (≈49.89 %, ≈36.00 % and ≈33.33 %, respectively). It has been reported that HaCaT is more susceptible to lysis than L929 cells when in contact with somewhat toxic substances [51]. Higher cell lysis percentages for SA and SA-NCMC hollow fibers may be related to their faster degradation profiles (release of many polymer fragments to the medium, which may block cell nutrient exchanges and other biological pathways essential to cell survival). In addition, the high hydrophilic character of the SA-based fibers and, hence, this polymer's great affinity towards water may limit protein adsorption [52]. Water molecules are the first to bind to a surface, paving the way for proteins to bind and generate surface recognition sites for cell attachment. If such event is conditioned, fibers' biocompatibility becomes compromised [53]. Because of its hydrophobic nature, the addition of PCL to the fibers decreased this effect. In fact, PCL and PCL-AAPV fibers presented the lowest cell lysis percentages for both cell lines (inferior to 10 %) along with the highest metabolic activity (higher than 70 %).

Many reports have shown that the addition of PCL to SA structures not only improves its biocompatibility but also leads to an increase in cell activity [52]. One possible explanation for such results may be related to the high structural integrity of such fiber typologies, which did not release polymer fragments and, therefore, caused no interference
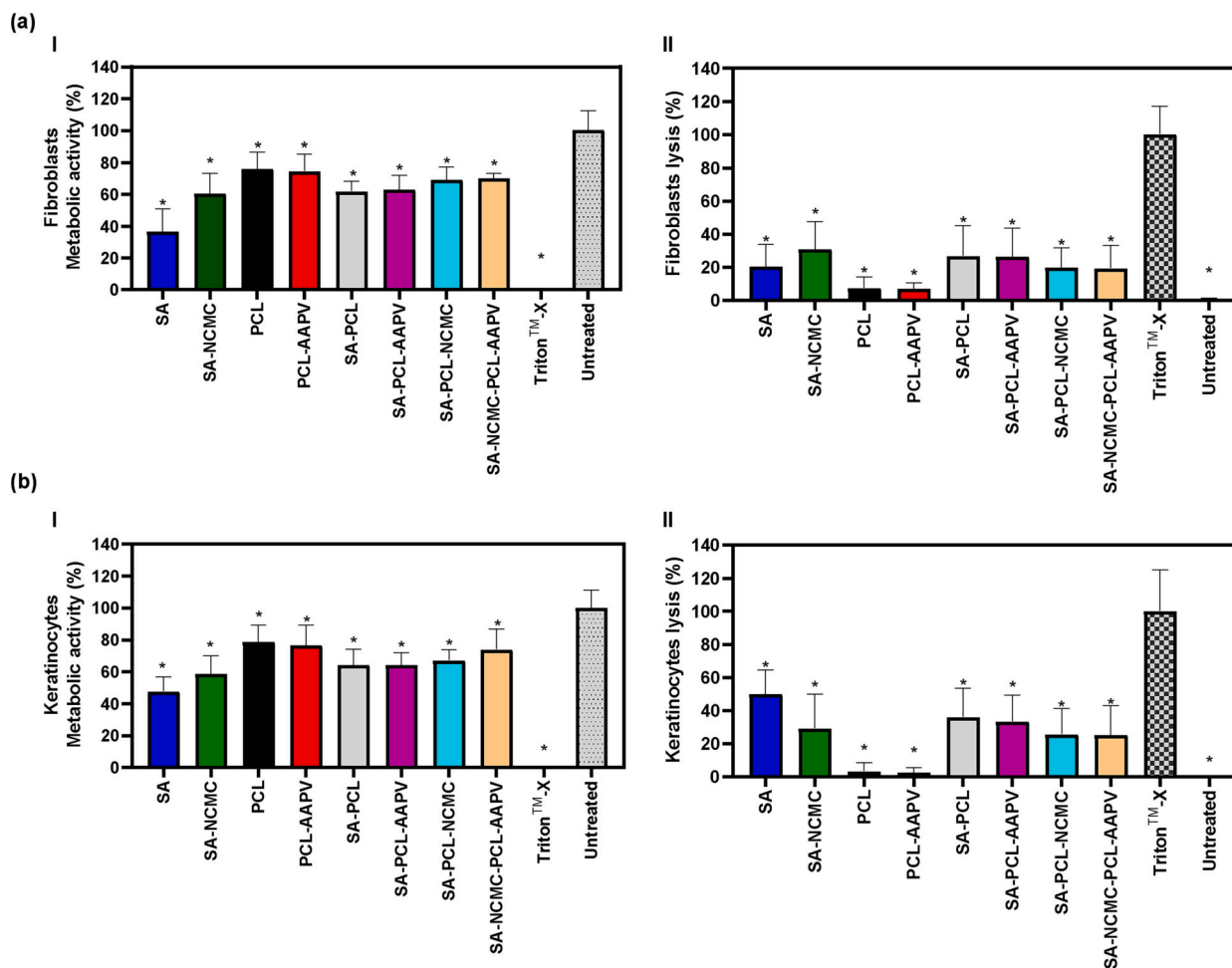
Fig. 9. Cytocompatibility evaluation: (a) fibroblasts from L929 and (b) keratinocytes from HaCaT cell lines were used to assess (I) the metabolic activity by resazurin assay and (II) cell lysis by LDH assay, after 24 h of direct contact with the wet-spun fibers. Data are reported as mean ± SD (n = 3). Statistical significance was determined via Dunnett test applying multiple comparisons between the different fiber typologies and each respective positive control (*p < 0.05).

with nutrient exchanges or other biological activities. Additionally, structures produced via wet-spinning technique are usually highly porous and present an interconnected porous structure, generating a large surface area, which features have been proven to promote cell attachment and proliferation [9].

PCL and PCL-AAPV fibers presented similar cell lysis, with differences between SA-PCL and SA-PCL-AAPV fibers and between SA-PCL-NCMC and SA-NCMC-PCL-AAPV fibers being also very reduced on this front. Such observations attest to the safety of the AAPV peptide and demonstrate its little influence on cells' metabolic activity. Although there are no reports on the cytocompatibility of AAPV, it is known that low molecular weight peptides loaded at small concentrations into scaffolding systems do not induce cytotoxic effects on cells [54]. On the other hand, the incorporation of NCMC was seen to improve the metabolic activity of both cells, compared to the NCMC-unloaded co-axial fibers. These results are consistent with several researches addressing the influence of CS derivatives, including NCMC, on mouse fibroblast-like cells [55]. To the authors' knowledge, CS mechanisms of action towards the metabolic activity of both cell lines are not yet fully understood. One hypothesis relies on the presence of cationic amine groups along the CS chains, which bind with anionic growth factors, consequently regulating their biological functions and affecting the metabolic activities of both tested cell lines [56]. According to Wen et al., CS binds

with anionic transforming growth factor-β (TGF-β), which promotes fibroblasts senescence, forming polyelectrolyte complexes. They reported that CS can downregulate the expression of TGF-β and delay cell senescence [57]. In general, all wet-spun fiber typologies guaranteed good cytocompatibility levels, which is in agreement with the literature [9].

3.13. Cell proliferation

Cell proliferation was evaluated by direct contact of all wet-spun fibers with L929 and HaCaT cell lines for 24 h and 48 h of incubation via the Hoechst staining method (Fig. 10). PCL and PCL-AAPV fibers promoted the highest cell proliferation for both cell lines. The contributions of PCL for cell attachment and proliferation are well described [52,58]. The explanations provided earlier to describe the PCL contributions to cell cytocompatibility can also be employed here, namely the superior structural integrity of PCL versus SA [53]. Additionally, wet-spinning, by generating structures with a rougher topography (increased porosity), may have allowed for more cells to bind and to establish strong interactions and, consequently, generate a supportive environment conducive to their proliferation.

Similarly to the results obtained from cell viability assays (Fig. 9), SA and SA-NCMC induced the lowest cell proliferation, most likely in
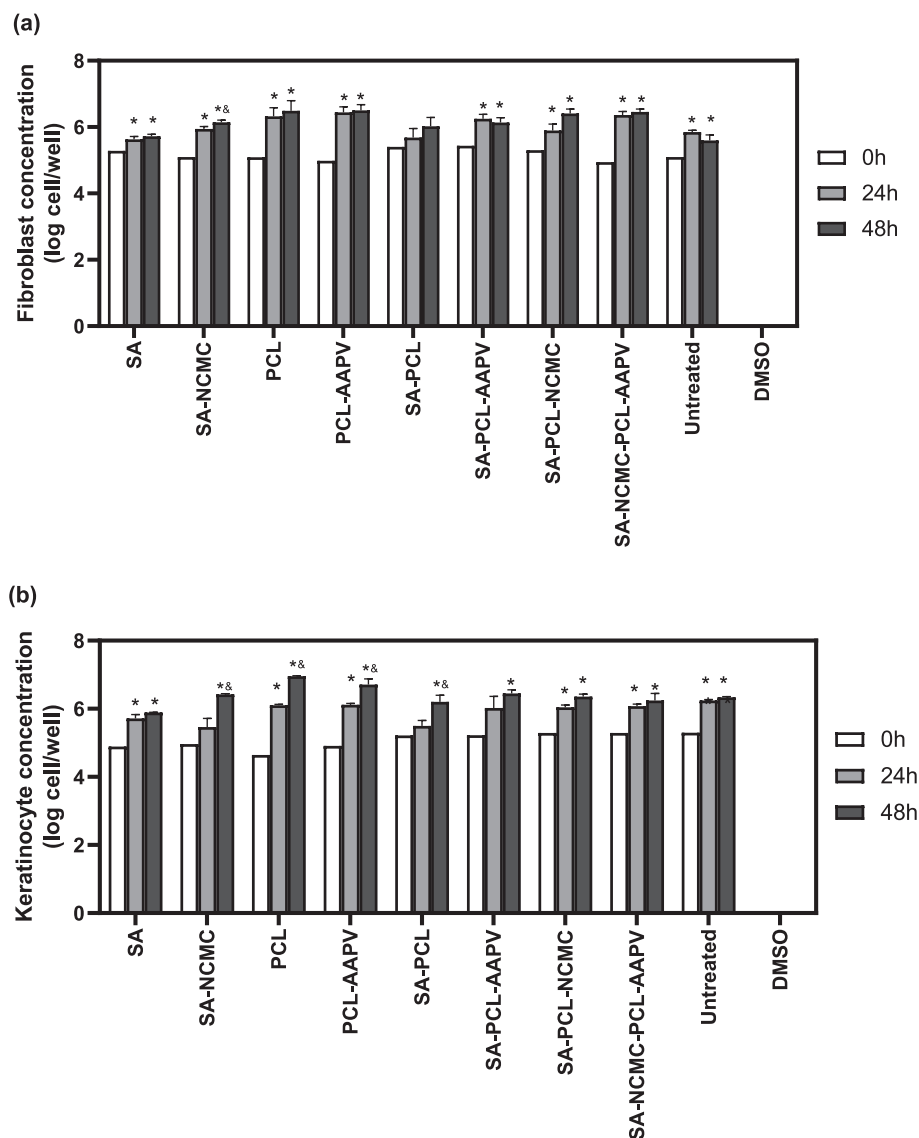
Fig. 10. Cell proliferation assessment: (a) fibroblasts from L929 and (b) keratinocytes from HaCaT cell lines were used to assess cell concentration by Hoechst staining at 0, 24, and 48 h of direct contact with the wet-spun fibers. Data are reported as cell concentration mean ± SD (n = 3). Statistical significance was determined via Tukey test applying multiple comparisons between the different fiber typologies (*p < 0.05, significant differences between 0 h and 24 h or 48 h testing; &*p < 0.05, significant differences between 24 h and 48 h testing).

response to the fibers' fast degradation and high hydrophilicity which may have compromised cell functions, protein surface adsorption, and subsequent cell attachment [52]. Moreover, NCMC-loaded co-axial fibers attained higher cell proliferation than SA-PCL and SA-PCL-AAPV fibers, attesting to this CS derivative enhancing effect on cell adhesion and proliferation [55].

Although there are no significant increments in cell proliferation during the first 24 h of incubation with both cell lines maintained their viable and well-defined morphologies after contact with all wet-spun fibers (Fig. S7 in Supporting Information), at the 48 h mark cell proliferation increased. This indicates that the slight negative effects induced on cell proliferation upon initial contact with the fibers were quickly overcome by the cells, potentiating these fibers' application for wound therapies longer than 24 h.

4. Conclusions

AAPV and/or NCMC-loaded co-axial wet-spun fibers were successfully produced for potential applications in the treatment of CW for a 24-hour period. Most wet-spun fibers maintained their structural integrity in physiological-like media, over time, revealing as well great elasticity and mechanical resilience; the only exception being the SA and SA-NCMC hollow fibers. These fibers were, however, endowed with excellent hydration capacity. Co-axial fibers guaranteed a controlled and prolonged release of AAPV, which HNE inhibitory action was proven effective. On its turn, NCMC-containing fibers were deemed antibacterial against *S. aureus*, particularly at the 6 h mark. Cytocompatibility evaluations confirmed the safety of the engineered fibers (also without inducing any alterations in cell morphology), while cell proliferation studies showed the fibers contribution to the increment in fibroblasts and keratinocytes numbers. Overall, this first report on co-axial wet-spun fibers for potential wound care therapies attested to the adequacy of the engineered system and demonstrated its ability to combine many intervention tools in one single structure. Future experimentation is still required to improve the scaffold's properties and will be performed to alter the structure of NCMC so its release can be more easily mapped, while also improving its antibacterial effectiveness. Moreover, AAPV synergisms with other bioactive molecules will need further exploration.

CRediT authorship contribution statement

Investigation, C.S.M., A.F.G.S. and C.L.S.; Data curation, C.S.M. and C.L.S; Writing - original draft preparation, C.S.M.; Writing - review and editing, C.L.S., S.R., M.M.P.S., S.M.M.A.P.-L., S.P.G.C., N.C.H., H.P.F.; Supervision, S.M.M.A.P.-L., S.P.G.C., N.C.H., H.P.F.; Funding acquisition, S.R., S.M.M.A.P.-L., S.P.G.C. and H.P.F. All authors have read and agreed to the published version of the manuscript.

Declaration of competing interest

The authors declare that they have no known competing financial interests or personal relationships that could have appeared to influence the work reported in this paper.

Data availability

No data was used for the research described in the article.

Acknowledgments

Appendix A. Supplementary data

Supplementary data to this article can be found online at https://doi.org/10.1016/j.bioadv.2023.213488.

References

[1] K. Järbrink, G. Ni, H. Sönnergren, A. Schmidtchen, C. Pang, R. Bajpai, J. Car, Prevalence and incidence of chronic wounds and related complications: a protocol for a systematic review, Syst. Rev. 5 (2016) 1–6, https://doi.org/10.1186/s13643-016-0329-y.

[2] L. Cañedo-Dorantes, M. Cañedo-Ayala, Skin acute wound healing: a comprehensive review, Int. J. Inflamm. 2019 (2019), https://doi.org/10.1155/2019/3706315.

[3] T.N. Demidova-Rice, M.R. Hamblin, I.M. Herman, Acute and impaired wound healing: pathophysiology and current methods for drug delivery, part 1: normal and chronic wounds: biology, causes, and approaches to care, Adv. Skin Wound Care 25 (2012) 304–314, https://doi.org/10.1097/01.ASW.0000416006.55218.d0.

[4] S.Y.C. Tong, J.S. Davis, E. Eichenberger, T.L. Holland, V.G. Fowler, Staphylococcus aureus infections: epidemiology, pathophysiology, clinical manifestations, and management, Clin. Microbiol. Rev. 28 (2015) 603–661, https://doi.org/10.1128/CMR.00134-14.

[5] M.A. Borg, L. Camilleri, What is driving the epidemiology of methicillin-resistant Staphylococcus aureus infections in Europe? Microb. Drug Resist. 27 (2021) 889–894, https://doi.org/10.1089/mdr.2020.0259.

[6] V. Patrulea, G. Borchard, O. Jordan, An update on antimicrobial peptides (Amps) and their delivery strategies for wound infections, Pharmaceutics. 12 (2020) 1–39, https://doi.org/10.3390/pharmaceutics12090840.

[7] Y.H. Ho, P. Shah, Y.W. Chen, C.S. Chen, Systematic analysis of intracellular-targeting antimicrobial peptides, bactenecin 7, hybrid of pleurocidin and dermaseptin, proline-arginine-rich peptide, and lactoferricin b, by using Escherichia coli proteome microarrays, Mol. Cell. Proteomics 15 (2016) 1837–1847, https://doi.org/10.1074/mcp.M115.054999.

[8] H.P. Felgueiras, M.T.P. Amorim, Functionalization of electrospun polymeric wound dressings with antimicrobial peptides, Colloids Surf. B: Biointerfaces 156 (2017) 133–148, https://doi.org/10.1016/j.colsurfb.2017.05.001.

[9] A. Mirabedini, Developing Novel Spinning Methods to Fabricate Continuous Multifunctional Fibres for A Thesis Submitted in the Fulfilment of the, 2017, pp. 1–235.

[10] I.R. Calori, G. Braga, P. da C.C. de Jesus, H. Bi, A.C. Tedesco, Polymer scaffolds as drug delivery systems, Eur. Polym. J. 129 (2020) 109621, https://doi.org/10.1016/j.eurpolymj.2020.109621.

[11] M. Umar, A. Ullah, H. Nawaz, T. Areeb, M. Hashmi, D. Kharaghani, K.O. Kim, I.S. Kim, Wet-spun bi-component alginate based hydrogel fibers: development and in-vitro evaluation as a potential moist wound care dressing, Int. J. Biol. Macromol. 168 (2021) 601–610, https://doi.org/10.1016/j.ijbiomac.2020.12.088.

[12] Q. Song, Z. Zhang, J. Gao, C. Ding, Synthesis and property studies of N-carboxymethyl chitosan, J. Appl. Polym. Sci. 119 (2011) 3282–3285, https://doi.org/10.1002/app.32925.

[13] H.C. Ge, D.K. Luo, Preparation of carboxymethyl chitosan in aqueous solution under microwave irradiation, Carbohydr. Res. 340 (2005) 1351–1356, https://doi.org/10.1016/j.carres.2005.02.025.

[14] I. Wiegand, K. Hilpert, R.E.W. Hancock, Agar and broth dilution methods to determine the minimal inhibitory concentration (MIC) of antimicrobial substances, Nat. Protoc. 3 (2008) 163–175, https://doi.org/10.1038/nprot.2007.521.

[15] European Society of Clinical Microbiology and Infectious Diseases, Broth dilution 2003, Clin. Microbiol. Infect. 9 (2003) 1–7.

[16] R. Alasbahi, M. Melzig, The in vitro inhibition of human neutrophil elastase activity by some yemeni medicinal plants, Sci. Pharm. 76 (2008) 471–484, https://doi.org/10.3797/scipharm.0804-25.

[17] J.V. Edwards, P. Howley, I.K. Cohen, In vitro inhibition of human neutrophil elastase by oleic acid albumin formulations from derivatized cotton wound dressings, Int. J. Pharm. 284 (2004) 1–12, https://doi.org/10.1016/j.ijpharm.2004.06.003.

[18] N.C. Homem, T.D. Tavares, C.S. Miranda, J.C. Antunes, M.P. Teresa, H.P. Felgueiras, Functionalization of Crosslinked Sodium Alginate / Gelatin Wet-spun Porous Fibers With Nisin Z for the Inhibition of Staphylococcus aureus - Induced Infections, (n.d.).

[19] F.C. Santos, A.M.S. Soares, M.S.T. Gonçalves, S.P.G. Costa, Phototriggered release of tetrapeptide AAPV from coumarinyl and pyrenyl cages, Amino Acids 49 (2017) 1077–1088, https://doi.org/10.1007/s00726-017-2405-6.

[20] A. Vasconcelos, N.G. Azoia, A.C. Carvalho, A.C. Gomes, G. Güebitz, A. Cavaco-Paulo, Tailoring elastase inhibition with synthetic peptides, Eur. J. Pharmacol. 666 (2011) 53–60, https://doi.org/10.1016/j.ejphar.2011.05.056.

[21] S. Namjoshi, I. Toth, J.T. Blanchfield, N. Trotter, R.L. Mancera, H.A.E. Benson, Enhanced transdermal peptide delivery and stability by lipid conjugation:

epidermal permeation, stereoselectivity and mechanistic insights, Pharm. Res. 31 (2014) 3304–3312, https://doi.org/10.1007/s11095-014-1420-5.

[22] J. Li, C. Cai, J. Li, J. Li, J. Li, T. Sun, L. Wang, H. Wu, G. Yu, Chitosan-based nanomaterials for drug delivery, Molecules. 23 (2018) 1–26, https://doi.org/10.3390/molecules23102661.

[23] X.G. Chen, H.J. Park, Chemical characteristics of O-carboxymethyl chitosans related to the preparation conditions, Carbohydr. Polym. 53 (2003) 355–359, https://doi.org/10.1016/S0144-8617(03)00051-1.

[24] Q. Jin, H. Yu, X. Wang, K. Li, P. Li, Effect of the molecular weight of water-soluble chitosan on its fat-/cholesterol-binding capacities and inhibitory activities to pancreatic lipase, PeerJ. 2017 (2017), https://doi.org/10.7717/peerj.3279.

[25] M.F. Queiroz, K.R.T. Melo, D.A. Sabry, G.L. Sassaki, H.A.O. Rocha, Does the use of chitosan contribute to oxalate kidney stone formation? Mar. Drugs 13 (2015) 141–158, https://doi.org/10.3390/md13010141.

[26] J. Li, S. Zhuang, Antibacterial activity of chitosan and its derivatives and their interaction mechanism with bacteria: current state and perspectives, Eur. Polym. J. 138 (2020) 109984, https://doi.org/10.1016/j.eurpolymj.2020.109984.

[27] R. Serra, R. Grande, L. Butrico, A. Rossi, U.F. Settimio, B. Caroleo, B. Amato, L. Gallelli, S. De Franciscis, Chronic wound infections: the role of Pseudomonas aeruginosa and Staphylococcus aureus, Expert Rev. Anti-Infect. Ther. 13 (2015) 605–613, https://doi.org/10.1586/14787210.2015.1023291.

[28] K. Apmann, R. Fulmer, A. Soto, S. Vafaei, Thermal conductivity and viscosity: review and optimization of effects of nanoparticles, Materials (Basel) 14 (2021) 1–75, https://doi.org/10.3390/ma14051291.

[29] I.L. Liakos, A. Mondini, E. Del Dottore, C. Filippeschi, F. Pignatelli, B. Mazzolai, 3D printed composites from heat extruded polycaprolactone/sodium alginate filaments and their heavy metal adsorption properties, Mater. Chem. Front. 4 (2020) 2472–2483, https://doi.org/10.1039/d0qm00159g.

[30] H.P. Felgueiras, N.C. Homem, M.A. Teixeira, A.R.M. Ribeiro, J.C. Antunes, M.T. P. Amorim, Physical, thermal, and antibacterial effects of active essential oils with potential for biomedical applications loaded onto cellulose acetate/polycaprolactone wet-spun microfibers, Biomolecules. 10 (2020) 1–20, https://doi.org/10.3390/biom10081129.

[31] A. Dodero, M. Alloisio, M. Castellano, S. Vicini, Multilayer alginate-polycaprolactone electrospun membranes as skin wound patches with drug delivery abilities, ACS Appl. Mater. Interfaces 12 (2020) 31162–31171, https://doi.org/10.1021/acsami.0c07352.

[32] A. Huang, Y. Jiang, B. Napiwocki, H. Mi, X. Peng, L.S. Turng, Fabrication of poly (ε-caprolactone) tissue engineering scaffolds with fibrillated and interconnected pores utilizing microcellular injection molding and polymer leaching, RSC Adv. 7 (2017) 43432–43444, https://doi.org/10.1039/c7ra06987a.

[33] A. Benkaddour, K. Jradi, S. Robert, C. Daneault, Grafting of polycaprolactone on oxidized nanocelluloses by click chemistry, Nanomaterials. 3 (2013) 141–157, https://doi.org/10.3390/nano3010141.

[34] A. de A. Morandim-Giannetti, P. de O. Wecchi, P. de A. Silvério, R. Carlstron, P. A. Bersanetti, Attainment and characterization of carboxymethyl chitosan hydrogels by enzymatic cross-linking, J. Therm. Anal. Calorim. 138 (2019) 3635–3643, https://doi.org/10.1007/s10973-019-08571-4.

[35] R.F.P. Pereira, J.P. Donoso, C.J. Magon, I.D.A. Silva, M.A. Cardoso, M. C. Gonçalves, R.C. Sabadini, A. Pawlicka, V. de Zea Bermudez, M.M. Silva, Ion conducting and paramagnetic d-PCL(530)/siloxane-based biohybrids doped with Mn2+ ions, Electrochim. Acta 211 (2016) 804–813, https://doi.org/10.1016/j.electacta.2016.06.088.

[36] S. Cai, T. Huang, H. Chen, M. Salman, K. Gopalsamy, C. Gao, Wet-spinning of ternary synergistic coaxial fibers for high performance yarn supercapacitors, J. Mater. Chem. A 5 (2017) 22489–22494, https://doi.org/10.1039/c7ta07937k.

[37] Y.B. Kim, G.H. Kim, PCL/Alginate Composite Scaffolds for Hard Tissue Engineering: Fabrication, Characterization, and Cellular Activities, 2014, https://doi.org/10.1021/co500033h.

[38] G.U. Rani, S. Sharma, Biopolymers, Bioplastics and Biodegradability: An Introduction, in: Ref. Modul. Mater. Sci. Mater. Eng, Elsevier, 2021, https://doi.org/10.1016/B978-0-12-820352-1.00131-0.

[39] M. Serhan, M. Sprowls, D. Jackemeyer, M. Long, I.D. Perez, W. Maret, N. Tao, E. Forzani, Total iron measurement in human serum with a smartphone, AIChE Annu. Meet. Conf. Proc. (2019), https://doi.org/10.1039/x0xx00000x, 2019-Novem.

[40] M.I. Wahba, Enhancement of the mechanical properties of chitosan, J. Biomater. Sci. Polym. Ed. 31 (2020) 350–375, https://doi.org/10.1080/09205063.2019.1692641.

[41] S.K. Bajpai, S. Sharma, Investigation of swelling/degradation behaviour of alginate beads crosslinked with Ca2+ and Ba2+ ions, React. Funct. Polym. 59 (2004) 129–140, https://doi.org/10.1016/j.reactfunctpolym.2004.01.002.

[42] L. Fan, Y. Du, B. Zhang, J. Yang, J. Zhou, J.F. Kennedy, Preparation and properties of alginate/carboxymethyl chitosan blend fibers, Carbohydr. Polym. 65 (2006) 447–452, https://doi.org/10.1016/j.carbpol.2006.01.031.

[43] K.Y. Lee, D.J. Mooney, Alginate: properties and biomedical applications, Prog. Polym. Sci. 37 (2012) 106–126, https://doi.org/10.1016/j.progpolymsci.2011.06.003.

[44] M. Rahman, J. Haider, T. Akter, M.S.J. Hashmi, Techniques for Assessing the Properties of Advanced Ceramic Materials, Elsevier, 2014, https://doi.org/10.1016/B978-0-08-096532-1.00124-2.

[45] Y. Wang, H. Chen, L. Cui, C. Tu, C. Yan, Y. Guo, Toughen and strengthen alginate fiber by incorporation of polyethylene glycol grafted cellulose nanocrystals, Cellulose. 29 (2022) 5021–5035, https://doi.org/10.1007/s10570-022-04601-x.

[46] J. Huang, C. Cui, G. Yan, J. Huang, M. Zhang, A study on degradation of composite material PBS/PCL, Polym. Polym. Compos. 24 (2016) 143–148, https://doi.org/10.1177/096739111602400209.

[47] H. Chopra, S. Bibi, S. Kumar, M.S. Khan, P. Kumar, I. Singh, Preparation and evaluation of chitosan/PVA based hydrogel films loaded with honey for wound healing application, Gels 8 (2022), https://doi.org/10.3390/gels8020111.

[48] R.C. Goy, D. De Britto, O.B.G. Assis, A review of the antimicrobial activity of chitosan, Polimeros. 19 (2009) 241–247, https://doi.org/10.1590/S0104-14282009000300013.

[49] Y. Xie, L. Yang, Calcium and magnesium ions are membrane-active against stationary-phase Staphylococcus aureus with high specificity, Sci. Rep. 6 (2016) 1–8, https://doi.org/10.1038/srep20628.

[50] M. Denda, Keratinocytes at the uppermost layer of epidermis might act as sensors of atmospheric pressure change, Extreme Physiol. Med. 5 (2016) 11–14, https://doi.org/10.1186/s13728-016-0052-2.

[51] A. Hoh, K. Maier, To Investigate Skin-irritating Substances, 1993.

[52] W.W. Hu, Y.C. Wu, Z.C. Hu, The development of an alginate/polycaprolactone composite scaffold for in situ transfection application, Carbohydr. Polym. 183 (2018) 29–36, https://doi.org/10.1016/j.carbpol.2017.11.030.

[53] H.P. Felgueiras, N.S. Murthy, S.D. Sommerfeld, M.M. Brás, V. Migonney, J. Kohn, Competitive adsorption of plasma proteins using a quartz crystal microbalance, ACS Appl. Mater. Interfaces 8 (2016) 13207–13217, https://doi.org/10.1021/acsami.5b12600.

[54] S. Chaiarwut, P. Ekabutr, P. Chuysinuan, T. Chanamuangkon, P. Supaphol, Surface immobilization of PCL electrospun nanofibers with pexiganan for wound dressing, J. Polym. Res. 28 (2021), https://doi.org/10.1007/s10965-021-02669-w.

[55] X. Li, X. Kong, Z. Zhang, K. Nan, L.L. Li, X.H. Wang, H. Chen, Cytotoxicity and biocompatibility evaluation of N,O-carboxymethyl chitosan/oxidized alginate hydrogel for drug delivery application, Int. J. Biol. Macromol. 50 (2012) 1299–1305, https://doi.org/10.1016/j.ijbiomac.2012.03.008.

[56] M. Ishihara, M. Fujita, K. Obara, H. Hattori, S. Nakamura, M. Nambu, T. Kiyosawa, Y. Kanatani, B. Takase, M. Kikuchi, T. Maehara, Controlled releases of FGF-2 and paclitaxel from chitosan hydrogels and their subsequent effects on wound repair, angiogenesis, and tumor growth, Curr. Drug Deliv. 3 (2006) 351–358, https://doi.org/10.2174/156720106778559047.

[57] C.W. Tsai, I.N. Chiang, J.H. Wang, T.H. Young, Chitosan delaying human fibroblast senescence through downregulation of TGF-β signaling pathway, Artif. Cells Nanomed. Biotechnol. 46 (2018) 1852–1863, https://doi.org/10.1080/21691401.2017.1394873.

[58] W.W. Hu, Y.T. Lin, Alginate/polycaprolactone composite fibers as multifunctional wound dressings, Carbohydr. Polym. 289 (2022) 119440, https://doi.org/10.1016/j.carbpol.2022.119440.